Osaamista
ja oivallusta
tulevaisuuden
tekemiseen

Daniel Hellsten

Liquid Metal Embrittlement in High Strength Steel Structures

Metropolia University of Applied Sciences

Bachelor of Engineering

Materials Technology and Surface Engineering

Thesis

31.10.2019

Author Title Number of Pages Date	Daniel Hellsten Liquid Metal Embrittlement in High Strength Steel Structures 37 pages + 5 appendices 31 October 2019
Degree	Bachelor of Engineering
Degree Programme	Biotechnology and Chemical Engineering
Professional Major	Materials Technology and Surface Engineering
Instructors	Arto Yli-Pentti, Senior Lecturer Esa Virolainen, Senior Specialist

The objective of this thesis was to examine hot-dip galvanized high strength steel structures with respect to liquid metal embrittlement. The objective included determination of a suitable inspection method for the detection of possible liquid metal induced cracking. Another objective was to determine a suitable etching method for the removal of the zinc layer from the surface of a hot-dip galvanized steel structure.

During the project hot-dip galvanized high strength steel structures were inspected to discover indications of possibly occurring liquid metal embrittlement. Examination methods for the detection of liquid metal assisted cracking were determined. Etching methods were examined for removal of zinc layer from surface of hot-dip galvanized high strength steel.

In this thesis the most critical parts of hot-dip galvanized high strength steel structures were examined with magnetic particle inspection and visual inspection to discover indications of possibly occurring liquid metal induced cracking. The removal of the zinc layer from the surface of high strength steel sample structures was conducted with a hydrochloric acid solution containing an inhibitor.

As a result of this thesis, no indications of liquid metal induced cracking in hot-dip galvanized high strength steel structures were detected with magnetic particle inspection or visual examination. Sodium hydroxide and hydrochloric acid are suitable for etching the zinc layer off the surface of a high strength steel structure.

The results provide information regarding the susceptibility of hot-dip galvanized high strength steel structures to liquid metal induced cracking. Magnetic particle inspection can be used in studies for detecting cracks in hot-dip galvanized steel structures. Results from the etching experiments could be utilized in studies where there is a need for removing the zinc layer from the surface of hot-dip galvanized steel structure.

Keywords	liquid metal embrittlement, high strength steel

Tekijä Otsikko Sivumäärä Aika	Daniel Hellsten Sulametallihauraus korkealujuuksisissa teräsrakenteissa 37 sivua + 5 liitettä 31.10.2019
Tutkinto	Insinööri (AMK)
Tutkinto-ohjelma	Bio- ja kemiantekniikka
Ammatillinen pääaine	Materiaali- ja pinnoitetekniikka
Ohjaajat	Lehtori Arto Yli-Pentti Vanhempi erikoisasiantuntija Esa Virolainen

Opinnäytetyön tavoitteena oli tutkia, esiintyykö kuumasinkitetyissä korkealujuuksisissa teräsrakenteissa merkkejä mahdollisesta kuumasinkityksen aiheuttamasta sulametallihauraudesta. Tavoitteena oli kartoittaa sulametallihaurauden aiheuttamien säröjen etsimiseen sopivia tutkimusmenetelmiä ja selvittää soveltuva syövytysmenetelmä sinkin poistamiseksi kuumasinkitetyn teräsrakenteen pinnalta.

Projektin aikana tutkittiin sulametallihaurauden esiintyvyyttä kuumasinkitetyissä korkealujuuksisissa teräsrakenteissa. Kartoitettiin tutkimusmenetelmiä sulametallihaurauden mahdollisesti aiheuttamien säröjen havaitsemiseksi kuumasinkitetyistä teräsrakenteista. Tutkittiin syövytysmenetelmiä sinkin poistamiseksi kuumasinkitetyn teräsrakenteen pinnalta.

Opinnäytetyössä tutkittiin kuumasinkitetyiden teräsrakenteiden sulametallihauraudelle alttiit alueet sulametallihaurauden mahdollisesti aiheuttamien säröjen löytämiseksi magneettijauhetarkastusmenetelmällä ja visuaalisella tarkastelulla. Sinkkikerroksen poisto teräksen pinnalta suoritettiin inhiboidulla suolahappoliuoksella.

Insinöörityön lopputuloksena saatiin havaintoja, joiden mukaan testatuissa kuumasinkitetyissä korkealujuuksisissa teräsrakenteissa ei esiintynyt sulametallihaurauteen viittaavia indikaatioita. Natriumhydroksidiliuos ja inhiboitu suolahappoliuos soveltuvat sinkin syövyttämiseen kuumasinkityn teräsrakenteen pinnalta.

Tulokset antavat tietoa testattujen kuumasinkitettyjen korkealujuuksisten teräsrakenteiden alttiudesta sulametallihauraudelle. Magneettijauhetarkastusmenetelmää voidaan käyttää säröjen kartoittamiseen kuumasinkitetystä teräsrakenteesta. Syövytyskokeiden tuloksia voidaan hyödyntää tutkimuksissa, joissa esiintyy tarve syövyttää sinkkikerros kuumasinkitetyn teräsrakenteen pinnalta.

Avainsanat	Sulametallihauraus, korkealujuuksinen teräs

Table of contents

Abbreviations

AHSS	Advanced High Strength Steel
CP	Complex Phase
DP	Dual Phase
EGGA	European General Galvanizers Association
EWHM	Enhanced Work Hardening Model
HSS	High Strength Steel
LMAC	Liquid Metal Assisted Cracking
LME	Liquid Metal Embrittlement
LMIE	Liquid Metal Induced Embrittlement
Q&P	Quench and Partitioning
RDC	Robinson Dissolution-condensation model
TBF	Transform Induced Plasticity Aided Bainitic Ferrite
TRIP	Transform Induced Plasticity
TWIP	Twinning Induced Plasticity
UHSS	Ultra High Strength Steel
UV	Ultra Violet
XRF	X-ray fluorescence

Appendices

1 Introduction

Development of high strength steels has been increasing due to its noticeable economic and environmental benefits. Advantages of high strength steels include possibilities to design lighter and more durable structures. Usage of high strength steels provides lower material costs and leads to reduced greenhouse emissions. In order to produce new advanced high strength steel products, long term development programs are necessary. This thesis was performed in co-operation with SSAB to contribute to the development of high strength steels by examining occurrence of liquid metal embrittlement in hot-dip galvanized high strength steel structures.

The objective of this thesis was to examine hot-dip galvanized structural steel (yield strength 900 MPa) structures considering liquid metal induced cracking. The topic for this thesis was chosen in order to get results to promote further development of hot-dip galvanized high strength steels. This thesis provides information considering the suitability of magnetic particle examination for the detection of cracks in hot-dip galvanized high strength steel structures. The results of the zinc etching experiments provide information regarding the removal of zinc layer from the surface of hot-dip galvanized high strength steel.

SSAB is a global steel manufacturer that is a leader in the world market in production of advanced high strength steels, quenched and tempered steels, and string, plate, and pipe products. SSAB develops high strength steels and offers services that strive to provide efficient and robust products. SSAB has production in Sweden, Finland and United States of America whose combined annual steel production capacity is approximately 8.8 million tons. The company is capable of handling and finishing different kinds of steel products in China, Brazil and some other countries. Production has been integrated into blast furnace processes in Finland and Sweden. Recyclable steel production process relies on arc furnaces in United States. SSAB was listed in Nasdaq in 1988, and its net sales in year 2018 were approximately 7 billion euros. [SSAB lyhyesti; Annual report 2018].

The history of SSAB starts in 1878 when steel mill Domnarvets Jerverk started operating. By the year 1972 factory was producing 500 000 tons of steel in a year. During that time numerous new facilities were founded for steel production. In 1978 Swedish state-

owned SSAB (Svensk Stål AB) was founded and ten years later in 1988 SSAB was enlisted to Nasdaq. In 2007 SSAB bought an American steel manufacturer IPSCO, and in 2010 the structure of the company was renewed by dividing it into three different geological business areas: EMEA (Europe, the Middle East and Africa), Americas and APAC (Asia-Pasific). In 2014 SSAB bought Rautaruukki Corporation and in 2016 SSAB, LKAB (Swedish State-owned mining company) and Vattenfall (Swedish electric company) set an aim for the future to produce the first fossil free steel manufacturing method. SSAB is an advocate of sustainable future and the objective of the company is to remove carbon dioxide emissions formed in manufacturing processes completely till year 2045. [Historia, SSAB:n Virstanpylväät].

2 Liquid metal embrittlement

Liquid metal embrittlement (LME) is a form of environmental cracking where a solid metal exposed to liquid metal has increased susceptibility to crack formation and propagation [Becker & Shipley 2002: 861]. LME involves brittleness or a loss of ductility and strength of a usually plastic material [Nilsson & Hojna 2018: 2; Vermeersch et al. 2011: 3]. This phenomenon is characteristic of specific solid-liquid metal couples such as steel-zinc and copper-quicksilver [Becker & Shipley 2002: 862]. It is commonly encountered in welding and hot-dip galvanization processes, where steel is being exposed to molten zinc and stress to metal structure is present [Vermeersch et al. 2011: 1]. Increased yield strength and hardening have been documented to increase LME susceptibility, predisposing high strength steels to this phenomenon [Nilsson & Hojna 2018: 5; Vermeersch et al. 2011: 1].

Several models propose that grain boundaries are crucial in advancement of LME and that LME normally involves penetration of the liquid metal along the grain boundaries of the solid metal. [Becker & Shipley 2002: 861]. It has been observed that even micrograms of liquid metal can induce embrittlement in 75 mm thick steel tubes [Cramer & Covino 2005: 381]. Embrittlement is observed as a reduction in fracture stress, strain or both, and fracture can occur well before the yield strength of the solid metal. The crack is usually brittle and it has been suggested that fracture stress varies with the inverse square foot of the average grain diameter of the metal. The fracture path is usually intergranular in polycrystalline metals having cubic center structure, and transgranular in hexagonial close-packed structures. Embrittlement is favored by barriers to

dislocation motion such as grain boundaries and precipitates; thus, pure metals and single crystals are less susceptible to embrittlement but not immune. High mutual solubility, high strength and grain boundary segregation have been recorded to increase LME susceptibility. [Becker & Shipley 2002: 861]. Velocity of crack propagation is around 10 to 100 cm/s. Due to fast crack growth rate, failure of small component is practically instant once an adequate stress is present. [Cramer & Covino 2005: 381].

2.1 Factors affecting LME

The embrittlement process during hot dip galvanizing is governed by multiple parameters and it is estimated that it would require understanding of up to 20 variables to declare an assured immunity to LME. Therefore a large number of input parameters are required for modeling of LME, leading in significant differences in results. Main variables affecting LME include microstructure, stress state, chemistry, and, environment. [Kohlman 2018: 1, 14]. Generally there are four influencing aspects (Picture 1) in which variables affecting LME cause modification in the hot-dip galvanization process. The first aspect is the mechanical and metallurgical condition of the steel. The second is the environment, including composition and temperature of the zinc bath. The third aspect is the acting forces, both residual and external stresses. The last aspect represents the influence of time, which refers to the zinc bath immersion time. [Vermeersch et al. 2011: 2].

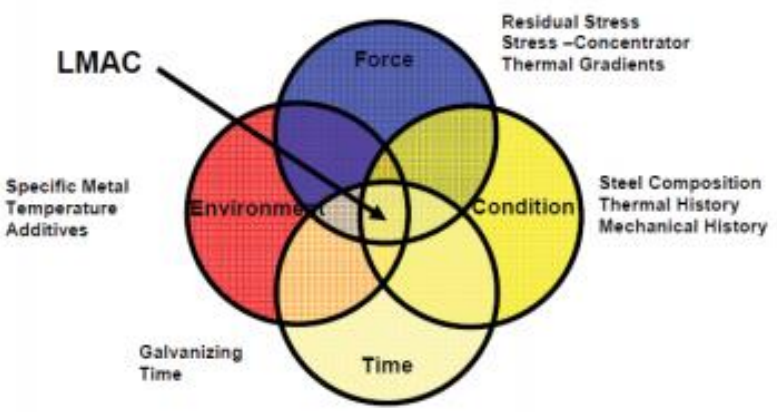

Picture 1. Four aspects influencing occurrence of LME. LMAC (liquid metal assisted cracking) is an alternative term for LME. [Vermeersch et al. 2011: 2].

The liquid metal embrittlement is not yet completely fully understood and theories explaining the phenomenon vary. Continuous research and advancement in theories considering LME have provided deeper knowledge on the subject. Theories considering LME can be categorized generally into two different categories. The first category includes theories regarding intra-atomic bonding, also known as adsorption. The second one contains theories on any other mechanisms, which usually involve mass-transport induced changes to geometric or mechanical properties of material. [Kohlman 2018: 1]. The main difference between models associated with the following: a) the assumed process for transport of atoms between the solid and liquid and b) the fracture process itself. All LME models assume that there is direct contact between the liquid and solid, which is the worst case scenario. [Nilsson & Hojna 2018: 8]. However, deficiencies between connecting atomistic simulations to macroscopic experimental results exist [Kohlman 2018: 1].

In order to model LME properly it is necessary to determine fracture controlling parameters. It is assumed that the volume directly affected by the embrittling atoms is localized to a very small region at the crack tip. Embrittling atoms affect physical properties that are expected to control embrittlement. These properties include surface energy of the solid, solid-liquid free surface, grain boundary energy, strength of interatomic bonds, cleavage stress, ideal shear strength, diffusion coefficient, mutual solubility, liquid and solid atoms in solid and the atoms in liquid. These parameters are very difficult to determine experimentally, but in the last decades there has been significant progress in computing from first principle calculations. Data regarding the modeling parameters is recorded in literature and databases. [Nilsson & Hojna 2018: 7].

2.2 Theories explaining LME

Theories considering intra-atomic bonding suggest that presence of adjacent liquid metal atoms affects interatomic bonding of solid-metal. The status of test conditions has been documented to have an effect on occurrence of LME. Increased temperature has been recorded to have an increased effect in occurrence of LME in welded, galvanized steel. Relatively high melting temperature of zinc enables enhanced diffusion of zinc to base metal in hot-dip galvanizing process. Kang et al. proposed that zinc penetration is controlled by stress-assisted solid-state diffusion on grain boundaries or mass transport of liquid Zn-Fe-Mn along grain boundaries. Material structure was observed to

have a significant effect on failure including grain boundary type and the grain size. [Kohlman 2018: 1, 2].

Reduction in surface energy model (RSE), based on Rebinder effect is one of the earliest models proposed considering LME. Model suggests that the free surface energy of the solid is reduced and classical Griffith approach can be applied for modeling of brittle fracture. A crack is formed when the stored elastic energy is released from crack extension and the work done by moving external surfaces equates the surface energy needed for the formation of new crack surfaces. A critical stress for a specific crack length can be determined by Equation 1. However Griffith approach is purely based on elastic deformation and does not regard for crack tip plasticity; therefore, the model is not currently extensively used in modeling of LME. [Nilsson & Hojna 2018: 8].

$$\sigma_c = \sqrt{\frac{E\gamma_e}{\alpha}} \quad \text{[Nilsson \& Hojna 2018: 8],} \qquad [1]$$

where σ_c is critical stress, E is Young`s modulus, γ_e is specific surface energy, and α is crack length.

Popvich and Dmukhovskaya have proposed an enhanced work hardening model (EWHM) that is based on enhanced dislocation emission by embrittling atoms. Model suggests that adsorbed embrittling atoms increase the number of slip planes leading in reduction of yield stress and increase in work hardening. As a result micro-cracks are formed at the surface, being located at various stress concentrators. [Nilsson & Hojna 2018: 16].

A model proposed by Robertson involves dissolution-condensation mechanism (DCM). In this model solid metal is dissolved into the liquid metal and solute diffuses trough the liquid metal away from the crack tip, leading on re-disposition of dissolved atoms on the crack surfaces. The process in mostly assumed to take place in the grain boundaries and slip planes with dislocation pile-ups. [Nilsson & Hojna 2018: 12].

3 Sources of stress

Stresses on material structure are one of the major aspects contributing to LME. Several manufacturing processes induce stress and residual stresses in structures. The

stresses result from cold working, hot-dip galvanization and thermal processes such as cutting and welding. In actual structures, stress concentrations such as grain boundaries, second phase particles and notches are capable of producing localized plastic deformation sufficient to cause LME cracking, and general plasticity is not necessary. [Vermeersch et al. 2011: 3].

3.1 Hot-dip galvanization

A structure is hot-dip galvanized to enhance its corrosion protection by immersing it to molten zinc bath. Zinc is metallurgically bonded with steel providing barrier separating oxidizing agents from substrate material. Zinc acts as a sacrificial anode to be oxidized instead of substrate material. When the zinc layer is damaged, zinc produces oxides that cover defects in zinc layer. [Vermeersch et al. 2011: 1].

In the hot-dip galvanization process the temperature of steel changes from the ambient temperature above the bath to the liquid zinc temperature and then back again. This variation in temperature causes thermal gradients in steel which induce stresses. The level of these stresses is a function of several parameters, of which the most important ones are dipping withdrawal speed and angle, structure geometry and bath composition. Preheating of steel and lowering bath temperature can reduce thermal gradients. [Vermeersch et al. 2011: 4]. In experiments LME susceptibility of steel increased as lead, tin and aluminum were added to zinc bath, tin content having the most significant effect on sensitivity to cracking. [Nygren 2015: 43, 44]. Low ductility and high strength of steel have been recorded to predispose the structure to suffer failure during galvanizing. Steelwork that is going to be hot-dip galvanized should not have high residual stresses or high stress concentrations; this can be achieved by rational design of large welded structures. Fluxing treatment is usually done to prevent oxidation before galvanizing and contributes to stress formation. Fluxing increases the surface roughness enhancing the susceptibility of local embrittlement due to notch effect which is related to stress concentration. [Ling et al. 2018: 8, 15].

3.2 Welding

Welding is a group of joining processes where parts are combined at their contacting surfaces by the application of heat and pressure. Welding processes are divided gen-

erally into two different categories; fusion welding and solid-state welding [Demeri 2012: 195]. Connecting steel structures by welding is efficient and economical. Welding does not require excessive holes in the parts to be connected and can be done without additional material such as plates and angles [Ram 2010: cp. 10, p. 1].

During the welding process a high temperature is induced to material causing the heat affected zone (HAZ) that is susceptible to LME [Ling et al. 2018: 35]. During welding process the maximum temperature of the joint varies from liquid steel temperature (over 1200 °C) to working temperature. Due to this, different types of heat effects are induced to the welding joint, producing zones with various microstructures, which mostly determine the strength of the welding joint. HAZ can be categorized into coarse granular, fine granular and partly austenitic zones. The most vulnerable zone considering impact strength is the coarse granular zone due to the high temperature (over 1100 °C). When steel is cooled down, the austenitic microstructure is dispersed leading in hard and usually ductile microstructures. Faster cooling rate leads to harder HAZ and increases crack susceptibility. [Lämsä & Kiuru 2012: 16]. It has been observed that during welding the maximum crack length increases with nugget diameter [Ling et al. 2018: 36]. The HAZ microstructure can be predicted by using a phase diagram e.g. Fe-Fe_3C phase diagram (Diagram 1) [Lippold 2014: 65].

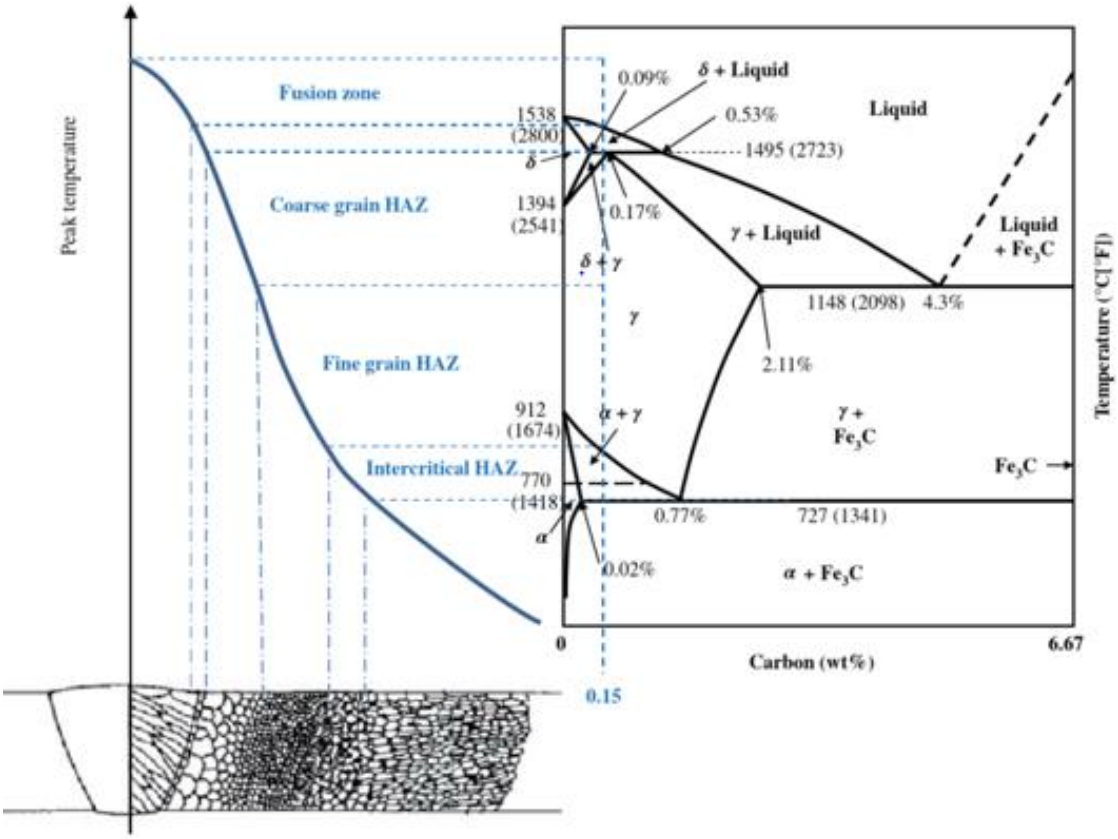

Diagram 1. Relationship between Fe-Fe_3C phase diagram and the microstructure in the HAZ of plain-carbon steels [Lippold 2014: 65].

Zinc`s melting point is surpassed in the galvanized steel welding process allowing solid-liquid contact [Ling et al. 2018: 35]. Because high strength steel (HSS) manufacturing process involves quenching, welding can induce a loss in HSS qualities due to heat convection. This can be reduced by limiting unnecessary heat convection during welding. [Lämsä & Kiuru 2012: 16]. Bruscato suggested that the zinc coating should be thoroughly removed from the joint area prior to welding to prevent LME cracking [Ling et al. 2018: 37]. The heat input during resistance spot welding of galvanized steels should be controlled by applying a proper welding procedure and welding parameters such as welding time, welding force and welding current [Ling et al. 2018: 35, 36, 39]. The static strength of welded structures depends on welding additives, welding technique, welding performance and placement of weld joints [Lämsä & Kiuru 2012: 16].

When using ultra high strength steels (UHSS) and abrasion resistant (AR) steels weld design and placement has to be more carefully planned compared to conventional steels. This considers choosing proper welding additives, takin into account fatigue strength of steel and placing welds on less stress concentrated locations. Structure of

the product should be practical and welds be designed so that the notch effect (e.g. sharp edges) remains minor. Corrects design of welds allows inspection of welds during and after welding procedure. [Lämsä & Kiuru 2012: 16].

4 High strength steels

Usage of high strength steels (HSS) has been increasing due to economic and environmental benefits [Kauppi & Kesti: 2016]. Yield strength of HSS is around 210 to 500 MPa and tensile strength is around 280 to 700 MPa. Steel types whose yield strength is over 550 MPa and whose tensile strength is over 700 MPa are referred to as ultra high strength steels (UHSS). [Lämsä & Kiuru 2012: 4]. The high strength and hardness of HSS is achieved by thermal processing, commonly hardening. The hardness of HSS is at least approximately 1.5 - 2.5 times higher than standard structural steels. [Kauppi & Kesti: 2016]. HSS provide lighter structure and are used in applications where high strength is required but there are limitations to structure`s weight. Reduced weight allows renovation of structures in which increasing amount of steel product customers are interested in. With elaborate design, weight of the steel structure can be reduced leading in lower material costs and reduced greenhouse emissions. [Busse et al. 2013: 5].

Price of HSS is higher than standard structural steels; however, reduction in material consumption leads to lower expenses. In automotive industry increased safety is achieved with HSS due to good energy absorption properties in a crash situation. The lighter structure of vehicles correlates directly to fuel consumption, leading in greater payload, reduced costs and reduced greenhouse emissions. [Busse et al. 2013: 5]. It is estimated that replacing conventional steel with AHSS in a typical vehicle will save approximately 2.2 tons of greenhouse gases over the vehicle`s life cycle, and carbon emissions could be reduced by 7.3 million tons if Europe`s recent vehicle base was updated to more modern cars, where advanced steel types are being applied [Demeri 2012: 259; Kauppi & Kesti 2016].

Increased design possibilities provided by lighter structure allow industrial manufacturers to design novel structures, leading in efficient manufacturing of industrial equipment. Using HSS and AR steels in parts that undergo high stress and are prone to wear increases overall lifetime of the product. Advantages of HSS have increased ap-

plication of them in many industrial fields. HSS are exploited in transportation vehicles, earthmoving vehicles, car cranes, forest machinery, process industry, cement and tree refinement, mining, and, mineral industry [Kauppi & Kesti: 2016: 4]. In order to mass-produce parts economically and efficiently high formability of HSS is required [Busse et al. 2013: 5]. This is achieved by attaining high state purity of steel, resulting in good cold-forming qualities [Lämsä & Kiuru 2012: 4]

4.1 Development of high strength steels

Steels are graded by manufacturers and users as they want because there is not standardized terminology [Kauppi & Kesti: 2016]. Steels can be categorized by manufacturing process or microstructural differences [Metalliteollisuuden keskusliitto 2001: 71]. Three generations of HSS have been developed, 3rd generation still being currently under development. Diagram 2 illustrates three generations of HSS location in stress-elongation curve [Busse et al. 2013: 8]. Each generation has been developed to provide enhanced qualities or to lower manufacturing costs. These advantages have been achieved by different manufacturing methods and modifications to steel microstructure. [Billur & Altan 2014: 1].

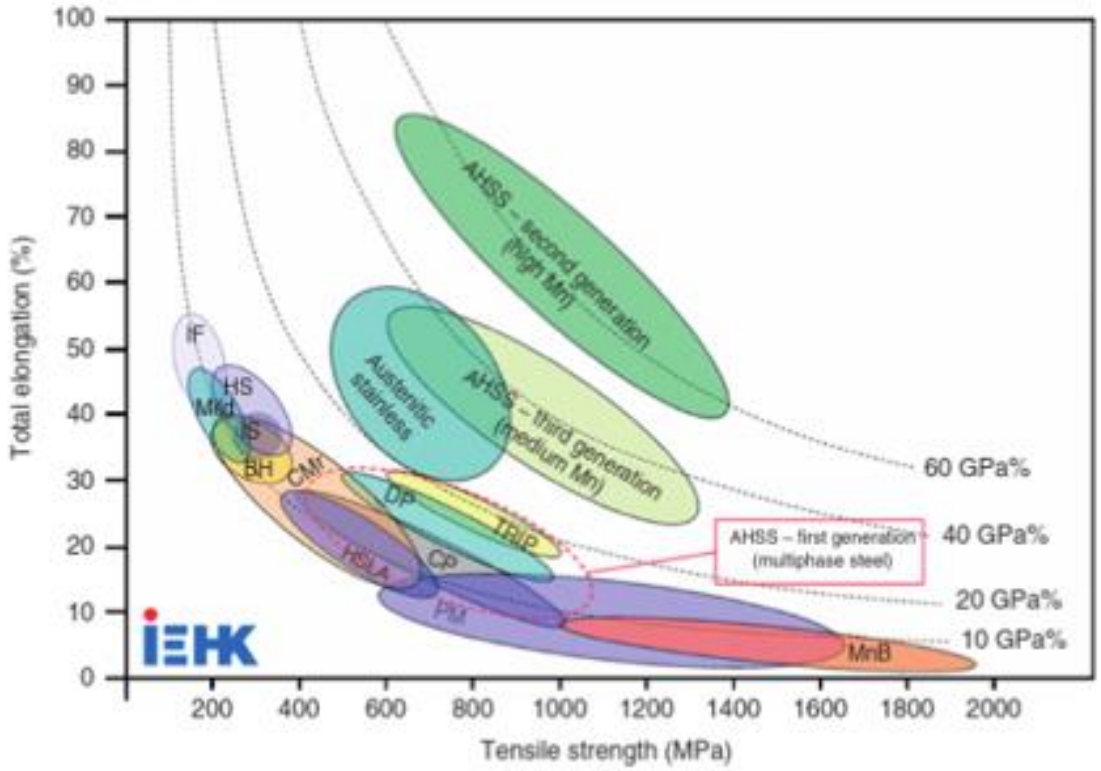

Diagram 2. Different generations of HSS in stress-elongation curve [Busse et al. 2013: 8].

4.2 1st generation of high strength steels

First generation advanced high strength steel (AHSS) has typically a martensitic microstructure, sometimes with one or more additional phases to improve formability. Dual phase (DP) steel is one of the most common type of AHSS which consist of ferritic and martensitic phases in order to achieve balance between formability and strength. Tensile strength of DP steels is around 590 to 1400 MPa. [Billur and Altan 2013: 1, 2].

Complex-phase (CP) steels contain bainite in addition to martensite and ferrite having higher formability than DP steels. Tensile strength of CP steels is between 800 to 1180 MPa. Martensitic steels (MS) are mostly martensitic containing small amounts of ferrite and bainite. MS have highest tensile strength (900 to 1700 MPa) but lowest elongation levels, leading in low formability. Press hardened steels have tensile strength of 1500 to 1800 MPa and are used extensively in safety and crash-resistant car body components. [Billur and Altan 2013: 1, 2].

4.3 2nd generation of high strength steels

Main difference between first and second generation of AHHS is development in austenitic microstructure, which affects in transformation induced plasticity (TRIP) [Billur et al. 2014: 1]. TRIP is a phenomenon where soft retained austenite is transformed into hard martensite during plastic deformation [Demeri 2012: 115]. This exhibits TRIP steels high strength and elongation, making TRIP steels suitable for energy absorption in car crash situations [Busse 2013: 20]. Diagram 3 illustrates TRIP steels energy absorption capacity compared to other AHSS [Schmitt & Iung. 2018]. The microstructure of TRIP steels consists of ferrite/bainite matrix and a 5 to 20 % volume fraction of metastable retained austenite which gradually transforms into martensite during plastic deformation. The transformation provides considerable dispersion hardening and resistance to localized deformation. [Demeri 2012: 115].

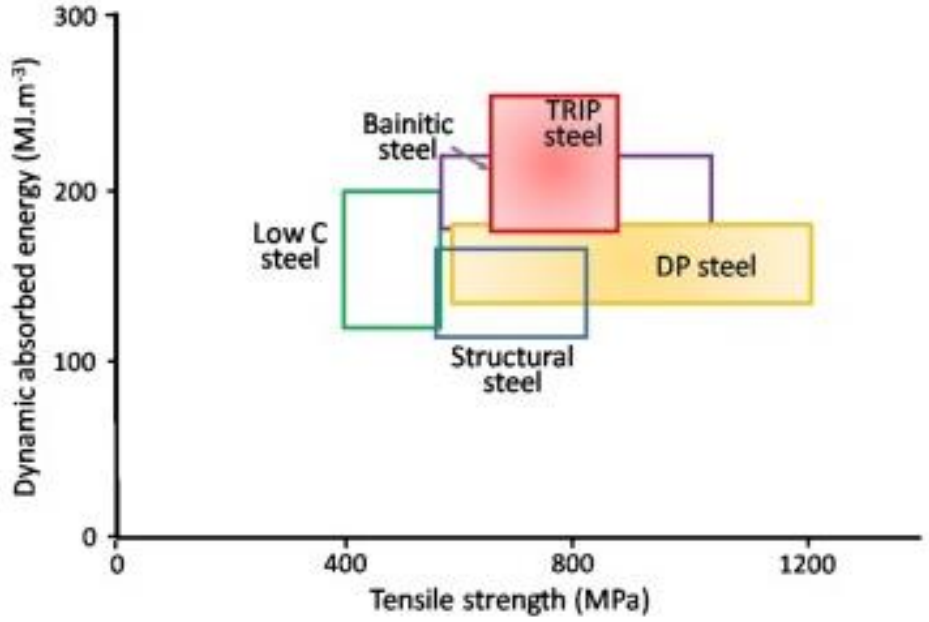

Diagram 3. AHSS Tensile strength - dynamic absorbed energy curve [Schmitt & Iung 2018].

Twinning induced plasticity (TWIP) is another strengthening mechanism. High-alloy elements (greater than 15 % manganese) cause formation of twins when steel is deformed. The twin boundaries act like grain boundaries to strengthen the steel. These steels typically have more than 50 % elongation at a strength level of about 1,000 MPa. Furthermore triplex steels are being developed having a very high manganese alloy content (15 to 30 %), among other elements. [Billur et al. 2014: 1].

4.4 3rd generation of high strength steels

First generation AHSS have limited formability and second generation AHSS have high strength and are more formable. However, second generation AHSS have tendency for delayed cracking and are relatively expensive because of their high-cost alloying elements. Third generation is being developed to offer high formability and strength at a reasonable cost. Two main types of 3rd generation steels that are currently produced are quenching and partitioning (Q&P) steels and transform induced plasticity aided bainitic ferrite (TBF) steels. The Q&P steel is composed of carbon, manganese and silicon alloying elements. Depending on strength level, amount of alloying elements can be as high as 4 %. During heat treatment of Q&P steel quenching is interrupted, and steel is reheated for partitioning. This creates structure consisting of 5 to 12 % stabile retained austenite, 20 to 0 % ferrite, and 50 to 80 % martensite. Q&P steel can have a tensile strength as high as 2100 MPa. [Billur & Altan 2014: 1].

TBF steels have reached yield strength of 980 MPa to 1470 MPa and are developed for spring back techniques and to prevent excessive necking. NanoSteel Corporation has developed a nanocrystalline steel structure that is achieved by refining austenite to nanometer scale after heat treatment. During plastic deformation stress-induced nanoscale phase formation increases strain hardening. [Billur & Altan 2014: 2].

5 Inspection methods

Visual inspection of steel structures is the most widely used inspection method of all time and many professional inspectors rely on it. With galvanized structures the crack is generally covered by a layer of zinc, so the crack may not be detected by visual inspection even when examined by experienced inspector. [Beldyk 2004: 1]. Nondestructive testing (NDT) methods have been developed to assist detection of defects not visible to eye, without removal of coating and causing damage to material. Zinc penetration to cracks and other reasons prevent usage of certain NDT methods such as dye penetrant testing and ultrasonic testing in examination of galvanized steel liquid metal induced cracking. [Beldyk 2014: 2]. Magnetic particle inspection and Eddy current testing can be used as NDT inspection methods for detection of liquid metal assisted cracking.

5.1 Magnetic particle inspection

Magnetic particle inspection is one of the oldest classical NDT inspection methods. It is the most used NDT inspection method after visual inspection when measured in number of pieces inspected. Method is applied especially in automotive industry for examination of safety elements. Technique exposes defects located on and adjacent to surface of ferromagnetic material. Cracks in size over 1 µm in width, 0.1 mm in depth and 1 mm in length can to be detected. The working mechanism is based on detection of leakages in magnetic field caused by defects in material. [SHY NDT-komitea magneettijauhetarkastus: 1, 11].

In magnetic particle inspection the part is magnetized causing magnetic field to distribute across a piece depending on permeability of magnetized material [SHY NDT-komitea magneettijauhetarkastus: 1]. Magnetization can be done by using permanent magnet or electromagnet [Portable Magnetizing Equipment for Magnetic Particle Inspection]. When a magnetized piece is broken into two pieces, both resulting pieces will form independent two-polar magnets. When the piece is not completely broken but damaged magnetic north pole and south pole are formed at each edge of cracks (Picture 2). When the magnetic field encounters foreign material in cracks (e.g. air, zinc) with alternative magnetic properties magnetic field is spread out. Leaking part of the magnetic field is called flux leakage field. Magnetic particles applied to surface of magnetized piece accumulate to flux leakage positions caused by defects on material (Picture 2). [Basic Principles].

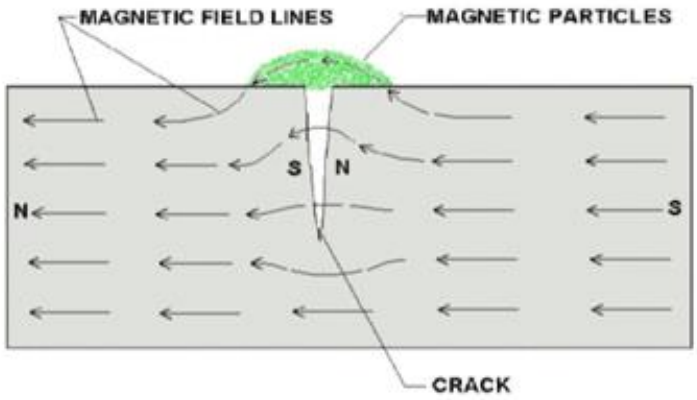

Picture 2. Formation of the magnetic south and north poles on edges of crack when magnetic field is induced to piece. Magnetic particle accumulation adjacent to crack due to flux leakage field [Basic Principles].

Magnetization is usually done by using permanent magnet or electromagnet. Usage of permanent magnets is not popular due to difficult removal of magnet and potential dangers involved placing the magnet. An electromagnetic yoke is a portable commonly used magnetization device, which involves a current to induce magnetic field (Picture 3). The current and thus also the magnetic field can be controlled with a switch. Other techniques to produce magnetization include cables and magnetization bench. [Portable Magnetizing Equipment for Magnetic Particle Inspection]. When magnetizing a piece for magnetic particle inspection, the intensity of magnetic flux inside of the piece has to be sufficient, thus too strong magnetic flux may lead to false indications [SHY NDT-komitea magneettijauhetarkastus: 2]. Magnetic field induced in the part must intercept the defect at a 45 to 90 degree angle to be clearly detected. Defects oriented perpendicular at 90 degree angle disrupt magnetic flux the most, producing strongest indications (Picture 3). [Portable Magnetizing Equipment for Magnetic Particle Inspection]. Magnetic particle inspection standard (SFS-EN ISO 9934-1:2016) suggests that coating thickness of over 50 µm reduces sensitivity of inspection [Mechanical Engineering and Metals Industry Standardization in Finland 2014: 6]. However cracks have been successfully detected when zinc coating thickness being approximately 100 µm [Rajala 2014: 42].

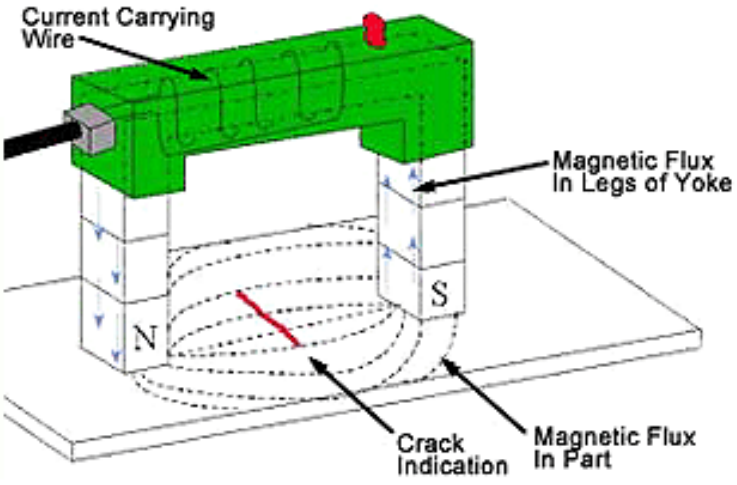

Picture 3. An electromagnetic yoke used in magnetic particle inspection and positioning towards crack [Portable Magnetizing Equipment for Magnetic Particle Inspection].

Applied particles are either dry particles or wet a suspension. Sensitivity of the wet suspension is higher than that of dry particles since particle movement in liquid is more effective. Particles with fluorescent properties are more effective indicating defects providing enhanced contrast for visual inspection. Correct pretreatment of examined surface is required for adequate results. Suspension is applied to surface before or during magnetization. After applying suspension, excessive examination fluid is let drain in order to prevent fading of indications. [Magnetic particles; Wet Suspension Inspection; SHY NDT-komitea magneettijauhetarkastus: 4, 6].

Particles used in fluorescence magnetic particle inspection are coated with a material that emits light in visible spectrum when exposed to ultraviolet light. Fluorescence is a phenomenon where a substance exposed to radiation emits radiation. Desired UV-light wavelength used for magnetic particle examination is between 3,500 and 3800 Angstroms. Hand held UV producing equipment is most commonly used. When beginning inspection with fluorescent particles, the inspector should take time for the eyes to adapt to lighting conditions to be able to detect clearly all indications. Special filtered glasses reflect potentially irritable UV-light but allow visible light to pass from fluorescent indicators making examination more precise. Standards considering lightning conditions during magnetic inspection have to be taken in to account for adequate results. [Lightning; Eye Consideration; Lights for Magnetic Particle Inspection].

5.2 Eddy current inspection

Eddy current testing is an NTD measurement technique based on Michael Faradays findings considering electromagnetic induction during early 1800`s [History of Eddy Current Testing]. Eddy current inspection is commonly used for surface examination of welds and pipes and for measurement of coating thickness of paint [SHY NDT-komitea Pyörrevirtatarkastus: 2]. It is also commonly used to conduct corrosion thinning measurements on aircraft skins and in the walls of tubing used in assemblies such as heat exchangers and steam generators [Tube Inspection; Thickness Measurements of Thin Material]. Cracks in size over 0.5 mm in width and 0.75 mm in length are possible to be detected by probe with multiple coils. Eddy current inspection provides advantages compared to magnetic particle inspection. The depth of crack can be measured and cleanness demand for examined surface is lower compared to magnetic particle inspection. [SHY NDT-komitea Pyörrevirtatarkastus: 2, 10].

Mechanism of action of Eddy current testing is following. An alternating current is applied to conductor by a coil, inducing a formation of magnetic field around the conductor. Magnitude of this primary magnetic field increases as the alternating current increases. When another electrical conductor is brought into the close proximity of changing magnetic field, current will be induced in the second conductor. Induced current will flow in a circular pattern and is called an Eddy current. The Eddy current produces a secondary magnetic field that is opposite to primary magnetic field. Defects such as cracks in conductive material disrupt the flow of the Eddy current, causing changes to secondary magnetic field and consequently to total magnetic field. Changes in total magnetic field induce changes to impedance of sensor`s coil and can be observed from screen of measurement instrument. [SHY NDT-komitea Pyörrevirtatarkastus: 1] Picture 4 illustrates Eddy current testing method layout and effect of defect on secondary magnetic field.

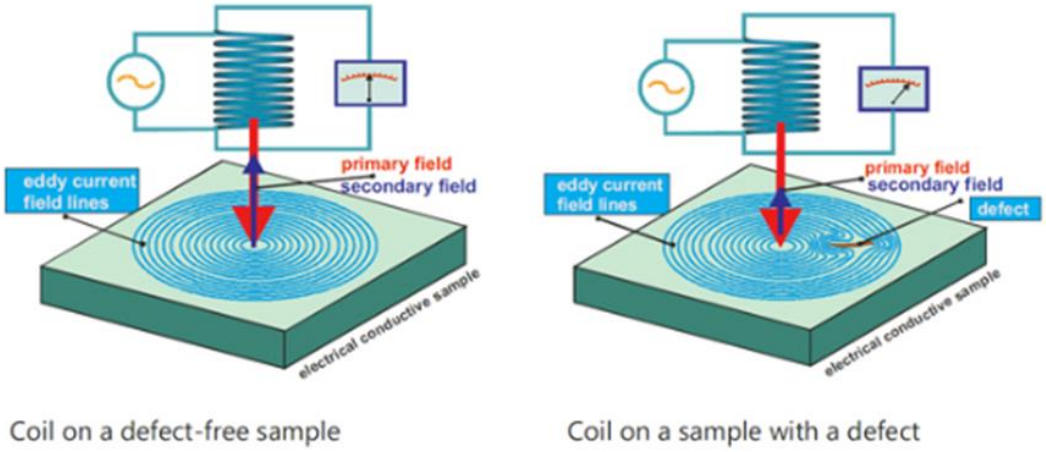

Picture 4. Arrangement of Eddy current testing method and effect of defect on secondary magnetic field [Eddy Current Principle].

Previously Eddy current inspection equipment was designed for specific objects. Currently equipment is designed to be versatile and suitable for different applications. Eddy current inspection probe consists of frame, one or several coils and interface. Connection to examined piece is achieved by primary and secondary magnetic field and physical connection is not necessary. Different types of probes are suitable for objects with

various geometry. [SHY NDT-komitea Pyörrevirtatarkastus: 3]. Picture 5 illustrates commonly used portable Eddy current inspection equipment and probe.

Picture 5. Portable Eddy current inspection equipment and probe [Equipment in ENSPL].

6 Initial experiments

6.1 Experiments with initial sample structures

Experiments with initial sample pieces were performed to test magnetic particle inspection method and equipment. The second objective was to investigate whether cracks induced to steel sheets would be detectable with magnetic particle inspection equipment after hot-dip galvanization.

Experiments were conducted with two initial sample sheets of high strength structural steel (yield strength 1100 MPa) provided by SSAB. The sheets had the following dimensions: thickness 8 mm, length 30 cm, width 25 cm. Cracks were intentionally induced to the sample steel sheets in the bending test by using a particularly small bending radius. The cracks covered by a zinc layer were noticeable to bare eye and with magnetic particle testing equipment. Bycorest cleaning products (Bycorest C 5, Bycorest C10) along Bycorest magnetic particle inks (Bycorest 101, Bycorest 14 HF) were tested, but noticeable difference between products was not detected. Hot-dip galvanization was done to initial sample pieces in the Material Surface Treatment Laboratory on the Myyrmäki campus of the Metropolia University of Applied Sciences (UAS). Hot-

dip galvanization was conducted to detect whether cracks would grow in size due to hot-dip galvanization process and to detect whether cracks would be detectable under the zinc layer with magnetic particle inspection equipment. The sample sheets were kept in zinc bath for 6 minutes and air-cooled after immersion. The elemental composition of zinc layer was measured from the surface of the hot-dip galvanized sample piece with an X-ray fluorescence (XRF) analyzer (Olympus Delta). The results of XRF measurements are illustrated in Table 1. Hot-dip galvanization was successfully completed and additional cracking was not observed, which is a notable result, considering bent and pre-cracked high strength steel samples (yield strength 1100 MPa).

Table 1. Results of X-ray fluorescence measurements from the surface of the hot-dip galvanized sample piece.

element	percentage (%)	variation (+/-)
Zn	98.1	0.03
Fe	0.66	0.01
Pb	0.41	0.02
S	0.349	0.008
Si	0.25	0.01
P	0.207	0.005
Mn	0.015	0.004
Ni	0.014	0.003

The surface thickness of the zinc layer was measured to be approximately 100 µm. Cracks were clearly observed through the zinc layer with visual inspection and magnetic particle inspection. Cracks were not observed to have grown in size after hot-dip galvanization with visual inspection or magnetic particle examination. Picture 6 illustrates the initial sample piece structure before hot-dip galvanization, and Picture 7 illustrates the same initial sample piece structure after hot-dip galvanization.

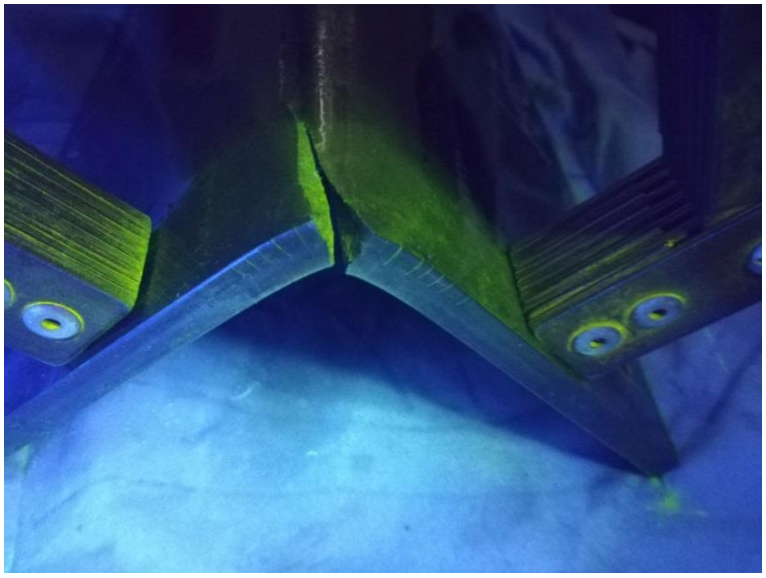

Picture 6. Initial sample piece structure before hot-dip galvanization when magnetic particle ink is applied to surface.

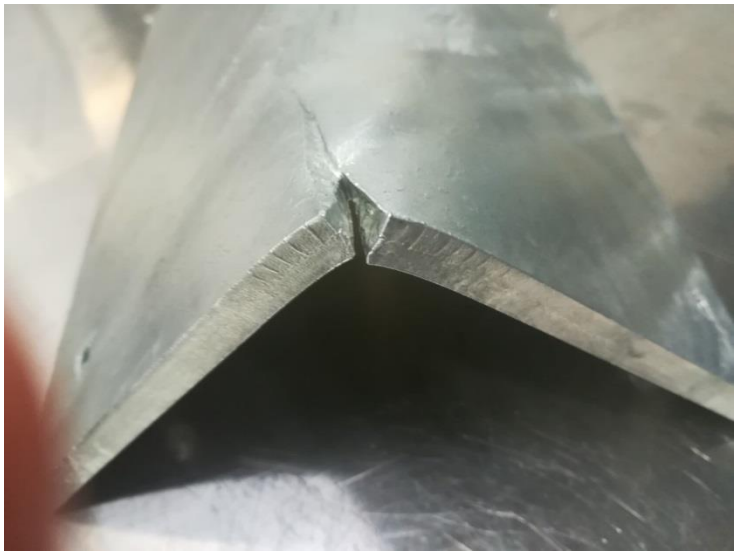

Picture 7. Initial sample piece structure after hot-dip galvanization.

6.2 Etching experiments of zinc layer

Etching experiments for the removal of the hot-dip galvanized zinc layer were conducted to detect which substances would be effective for purpose. Removal of the zinc layer from the surface of the hot-dip galvanized high strength steel structure could be beneficial when conducting experiments where cracks in hot-dip galvanized steel structure are required to be detected.

For the etching experiments eight sample pieces of approximately 5 x 5 cm in size were cut from high strength steel (yield strength 1100 MPa, steel sheet thickness 6 mm) structures that were hot-dip galvanized in previous experiments of this project in the Material Surface Treatment Laboratory of Metropolia UAS. Four different kinds of solutions were prepared for experiments, two of each kind to test their zinc dissolving capabilities. Each of eight hot-dip galvanized steel pieces was immersed in separate beakers filled with different solutions and surface thickness of samples was periodically measured as time proceeded. The following solutions used in the etching experiments: NaOH 25 %, NaOH 50%, NH_4NO_3 12 % and HCl 16.5 % + inhibitor (Rodine 60, contains 20 - 40 % of hexamethyltetramine) 0.5 %. The labeling of solutions used in the etching experiments is illustrated in Table 2.

Table 2. Solutions of zinc etching experiments.

Solution 1	Sample 1	NaOH 25 %
Solution 2	Sample 2	NaOH 25 %
Solution 3	Sample 3	NaOH 50 %
Solution 4	Sample 4	NaOH 50 %
Solution 5	Sample 5	NH4NO3 12 %
Solution 6	Sample 6	NH4NO3 12 %
Solution 7	Sample 7	HCl 16.5 % + inhibitor 0.5 %
Solution 8	Sample 8	HCl 16.5 % + inhibitor 0.5 %

Surface thickness and mass of hot-dip galvanized steel samples were measured in the beginning of experiment before immersing samples into solutions. Surface thickness and mass of samples were measured at 2, 4, 24 and 48 hours after the beginning of experiment. Samples 5 and 6 etched with NH_4NO_3 were kept immersed in solutions for a longer time due to minor changes noticed in the surface thickness of samples. Surface thickness of Sample 5 was measured in 168 hour time mark and the surface thickness of Sample 6 was measured at 144 hours. 10 readings per sample were taken with a surface thickness measurement device (Elcometer 456) each time surface thickness of samples was measured. Surface thickness measurements of the sample pieces during the etching experiment are listed in Table 3 and illustrated in Diagram 4. Mass measurements of the sample pieces during etching experiment are listed in Table 4 and illustrated in Diagram 5.

Table 3. Surface thickness measurements of sample pieces during etching experiment. Each value of surface thickness in the chart is an average of 10 repeated measurements.

Sample 1 NaOH 25 %		Sample 2 NaOH 25 %		Sample 3 NaOH 50 %		Sample 4 NaOH 50%	
time (h)	surface thickness (µm)	time (h)	surface thickness (µm)	time (h)	surface thickness (µm)	time (h)	surface thickness (µm)
0	102.15	0	77.21	0	83.37	0	100.03
2	98.82	2	67.26	2	72.08	2	85.78
4	91.76	4	72.55	4	65.48	4	79.86
24	9.41	24	7.72	24	2.57	24	3.25
48	1.84	48	2.46	48	1.89	48	1.44
Sample 5 NH4NO3 12 %		**Sample 6 NH4NO3 12 %**		**Sample 7 HCl 16,5 %, inh. 0,5 %**		**Sample 8 HCl 16,5 %, inh. 0,5 %**	
time (h)	surface thickness (µm)	time (h)	surface thickness (µm)	time (h)	surface thickness (µm)	time (h)	surface thickness (µm)
0	104.41	0	90	0	94.25	0	82.42
2	110.5	2	96.38	2	1.7	2	1.38
4	100.8	4	91.57	4	1.44	4	1.89
24	110.88	24	89.98	24	1.7	24	1.6
48	107.19	48	91.8	48	1.68	48	1.55
168	113.86	144	105.67				

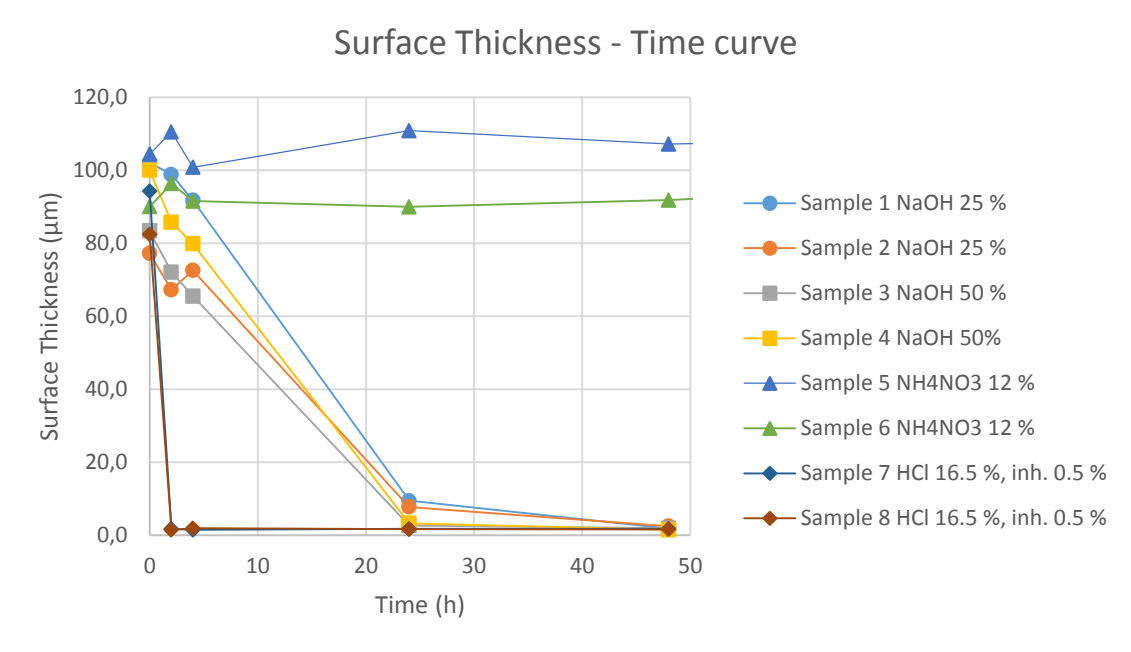

Diagram 4. Surface thickness - Time curve. Composed of surface thickness measurement data presented in Table 3. Time axis is limited to 50 h. Figure composed of equivalent measurement data extended to display time till 180 h is illustrated in appendix 1.

Table 4. Mass measurements of sample pieces during etching experiment.

Sample 1 NaOH 25 %		Sample 2 NaOH 25 %		Sample 3 NaOH 50 %		Sample 4 NaOH 50%	
time (h)	mass (g)	time (h)	mass (g)	time (h)	mass (g)	time (h)	mass (g)
0	144.111	0	145.401	0	147.829	0	151.879
2	145.154	2	143.83	2	147.466	2	151.487
4	143.743	4	145.087	4	147.294	4	151.323
24	142.111	24	143.759	24	145.837	24	149.837
48	141.428	48	143.025	48	145.418	48	149.384
Sample 5 NH4NO3 12 %		**Sample 6 NH4NO3 12 %**		**Sample 7 HCl 16,5 %, inh. 0,5 %**		**Sample 8 HCl 16,5 %, inh. 0,5 %**	
time (h)	mass (g)	time (h)	mass (g)	time (h)	mass (g)	time (h)	mass (g)
0	145.797	0	158.544	0	151.712	0	147.922
2	145.736	2	158.473	2	148.458	2	144.843
4	145.712	4	158.436	4	148.445	4	144.821
48	145.652	24	158.385	24	148.335	24	144.73
168	145.529	48	158.36	48	148.248	48	144.644
		144	158,27				

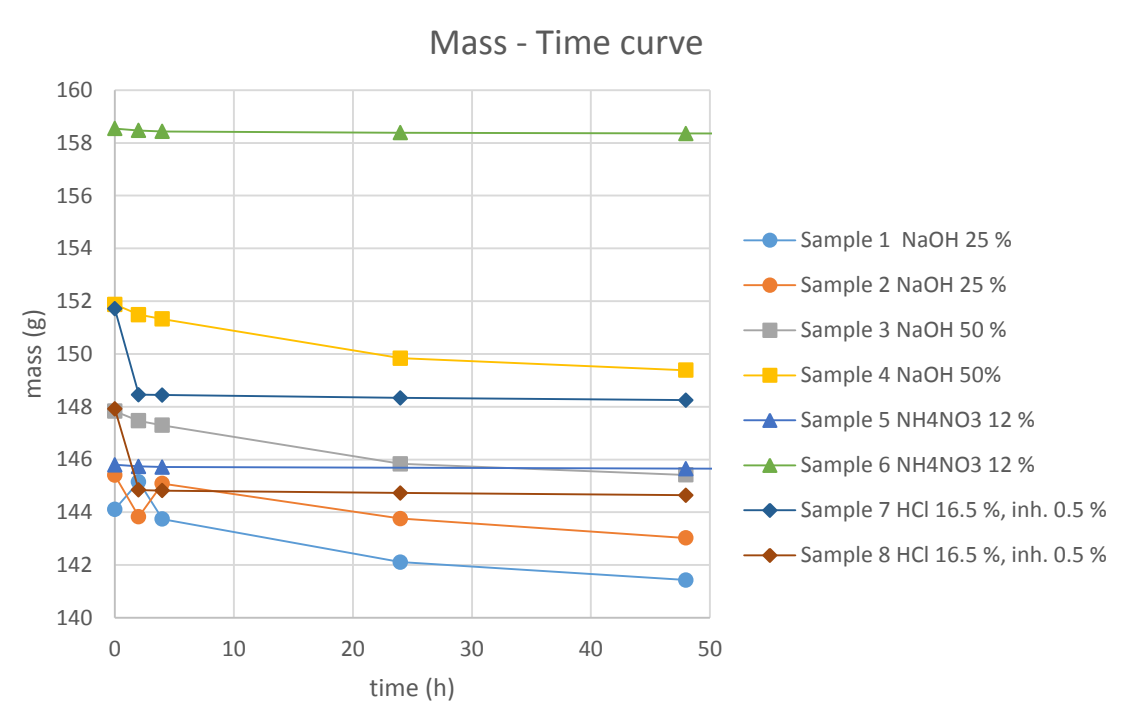

Diagram 5. Mass - Time curve. Composed of mass measurement data presented in Table 4. Time axis is limited to 50 h. Figure composed of equivalent measurement data where time axis is extended to display time till 180 h illustrated in appendix 1.

Clear reduction in mass and surface thickness was observed in samples etched with NaOH 25 %, NaOH 50% and HCl 16.5 % containing 0.5 % of inhibitor. Significant reduction in surface thickness or mass in samples etched with NH_4NO_3 was not observed. Results of surface thickness measurements are in line with mass measurements as mass reduction was observed as surface thickness of pieces reduced. Solutions containing NaOH 25 % and NaOH 50 % seemed to be equally effective when taking in the account differences in surface thickness of samples in the beginning of experiment. NaOH 25 % and NaOH 50 % etched zinc virtually completely in 24 hours. HCl 16.5 % containing 0.5 % of inhibitor was the most effective, having etched zinc completely in two hours. Surface thickness of samples etched with NH_4NO_3 stayed approximately the same and was observed to have slightly increased over time. Slight increase in surface thickness of samples etched with NH_4NO_3 was observed in two hour mark while significant change in mass was not observed.

Reaction with zinc and sodium hydroxide is following (reaction 1). Hydrogen is formed in this reaction, therefore using inhibitor to prevent hydrogen embrittlement could be justifiable.

$Zn + 2\ NaOH \rightarrow Na_2ZnO_2 + H_2$ (reaction 1)

HCl dissolves zinc in reaction 2 forming hydrogen gas that could be detrimental to structure. Therefore inhibitor is added to prevent hydrogen embrittlement.

$Zn + 2\ HCl \rightarrow ZnCl_2 + H_2$ (reaction 2)

7 Experimental part

7.1 Modeling of sample pieces with computer assisted software

The basic-model of sample pieces with dimensions was given by SSAB to be modeled with computer assisted software. Model of sample piece was designed to represent different kind of structural features that were regarded to be prone to liquid metal embrittlement. Such features involved welds, bends and different kind of shaped cuts. Altogether four samples were planned to be manufactured, two to be cut with plasma and two to be cut with laser. Differently shaped lightening holes were designed on

sides of sample parts and a suspension hole for hot-dip galvanization was designed on the upper corner of each structure. To separate plasma cut samples from laser cut samples a small notch was designed in the corner of laser cut samples. Pictures 8, 9, 10 and 11 illustrate 3D-design of sample structures designed with Solidworks. The thickness of the steel sheet used for manufacturing of parts is 6 mm. Rounding radius of lightening holes edges is 20 mm. Bending radius of structures is 21 mm = 3.5 t. Dimensions of samples are illustrated in Appendix 2 which contains complete 2-D blueprints of samples.

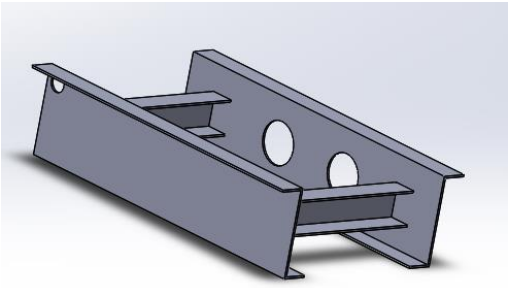

Picture 8. 3-D model of Sample 1 designed with Solidworks (plasma cut).

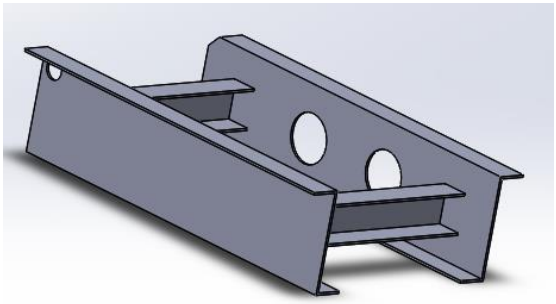

Picture 9. 3-D model of Sample 2 designed with Solidworks (laser cut).

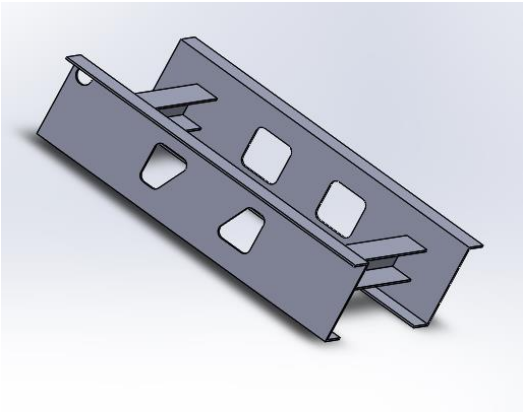

Picture 10. 3-D model of Sample 1 designed with Solidworks (laser cut).

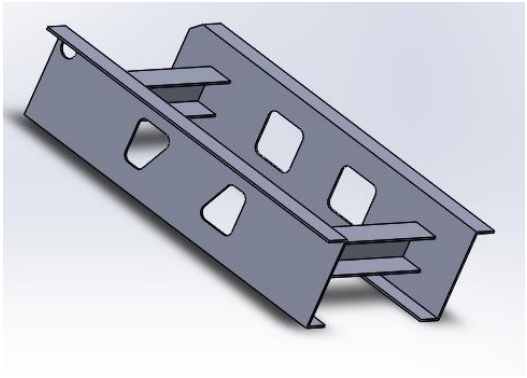

Picture 11. 3-D model of Sample 3 designed with Solidworks (plasma cut).

Each sample piece was manufactured from four separate steel parts by welding them together. SSAB`s subcontractors have programmable plasma and laser cutting devices which could cut shapes automatically based on blueprints that were input to the equipment software. Therefore, 2-D spread blueprints (appendix 3) of steel plates were de-

signed with Solidworks and the file type was converted to DXF-file that was a compatible file format to be input to the software of the programmable cutting equipment.

7.2 Manufacturing of sample pieces

Sample pieces were manufactured from structural high strength steel (yield strength 900 MPa) whose elemental composition is illustrated in Table 5. Steel sheets were cut with plasma and laser cutting equipment according to 2-D spread blueprints (Appendix 3). Each sample piece was manufactured from four separate sheets of steel that were welded together. Picture 12 illustrates composed steel structures after welding in SSAB`s facilities. The bending radius of structures was originally planned to be 36 mm but was changed to 20 mm by bending expert of SSAB. Bending radius of 20 mm was confirmed with press to have been successfully actualized (Picture 13). Surfaces of the rolled areas were checked to be Class 1 and 2 being approvable quality, some having shape slightly resembling a nut. The actual dimensions of pieces differed slightly from the originally designed dimensions. Two main changes to the actual dimension are illustrated in Picture 14.

Table 5. Elemental composition of examined high strength structural steel (yield strength 900 MPa).

element	percentage (%)
C (max. %)	0.1
Si (max. %)	0.25
Mn (max. %)	1.3
Al Tot (min. %)	0.015
Nb (max. %)	0.05
V (max. %)	0.05
Ti (max. %)	0.07

Picture 12. Composed steel structures after welding and cutting.

Picture 13. Confirmation of rolling radius of 20 mm with press.

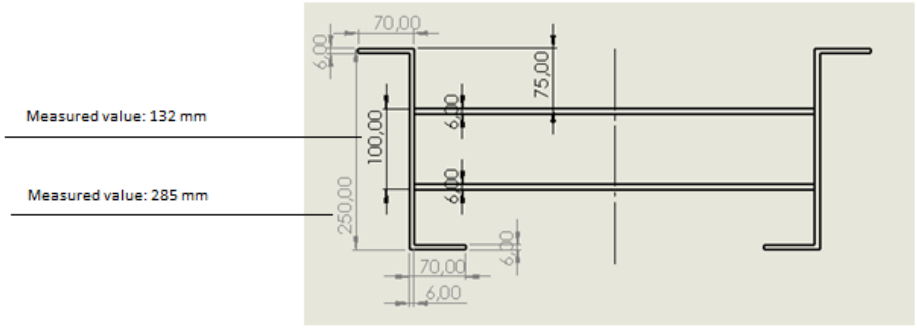

Picture 14. Actual dimensions compared to originally designed dimensions.

7.3 Hot-dip galvanization of sample structures

After composing of sample structures, the structures were delivered to Aurajoki Corporation facilities in Pirkkala to be hot-dip galvanized. Before hot-dip galvanization additional holes with radius of 10 mm were drilled into structures by SSAB. The holes were drilled in accordance with the recommendation of Aurajoki Corporation to enhance dripping of zinc when hot-dip galvanizing the structures. For hot-dip galvanization the

pieces were suspended the way illustrated in Picture 15. During the hot-dip galvanization process all pieces remained without visible damage. This was a desirable result since heat variations during immersion due to molten zinc induce stresses to structure, which could result to tearing.

Picture 15. Sample structures suspended for hot-dip galvanization.

Degreasing was performed in acidic degreasing solution. Pickling was performed in an HCl bath containing an inhibitor for 3 hours. After rinsing and fluxing the sample pieces were dried at 75 °C in an oven approximately for half an hour. Pieces were kept in an oven which functioned as a preheating treatment to reduce the heat shock during the immersion to zinc. Zinc bath immersion time was 3-4 minutes, typical bath time being 2-3 minutes. Pieces were descended at the fastest speed that lifter moved though the speed was undefined. The pieces were moved around at the beginning of dipping to reduced ash marks on the surface of the pieces. Bismuth and tin were mixed in the bath. Lead was not added to the bath but it was included as a natural impurity of zinc.

European General Galvanizers Association (EGGA) has set recommendations for limits of element concentrations in galvanization bath to avoid liquid metal induced cracking. For galvanizing of constructional steel, where high levels of component strain are not present during dipping, it is recommended that, in addition to the requirements of standard EN ISO 1461, the combined levels of tin, bismuth and lead shall not exceed 1.0 %. For galvanizing of steel structures more susceptible to liquid metal embrittlement, limits for certain element concentrations are even tighter (Table 6). Galvanization

bath that was used for galvanizing sample pieces fulfilled these recommendations of EGGA for element concentrations. [EGGA 2014: 6].

Table 6. European General Galvanizers Association`s recommended limits of element concentrations in galvanization bath for structures more susceptible to liquid metal embrittlement [EGGA 2014: 6].

	Maximum composition in galvanizing bath (wt%)
Sn	≤ 0.1%
Pb + 10Bi	≤ 1.5%

After hot-dip galvanization, pieces were shipped to Metropolia University of Applied Sciences in Myyrmäki Vantaa to be examined. Surface thickness of zinc layer was measured from Sample 3 with nondestructive surface thickness measurement device (Elcometer 456) to be approximately 100 µm. Two-point calibration was used in the calibration of the surface thickness measurement device. Complete surface thickness measurements of Sample 3 are illustrated in Appendix 4.

7.4 Magnetic particle examination of sample structures

Before magnetic particle examination, all specimens were labeled and marked to enable systematic inspection of samples. Each end of the long part of structures were labeled and marked in a following manner: A, B, C, D when suspension hole facing up (Picture 16). All pieces were cut in half by cutting middle bars of the structures in half from the middle with angle grinder. This enabled better access to examine desired areas of the structures. Locations of cutting spots were determined to be far enough from examined sections in order to prevent heat effect from cutting to impact the areas to be examined.

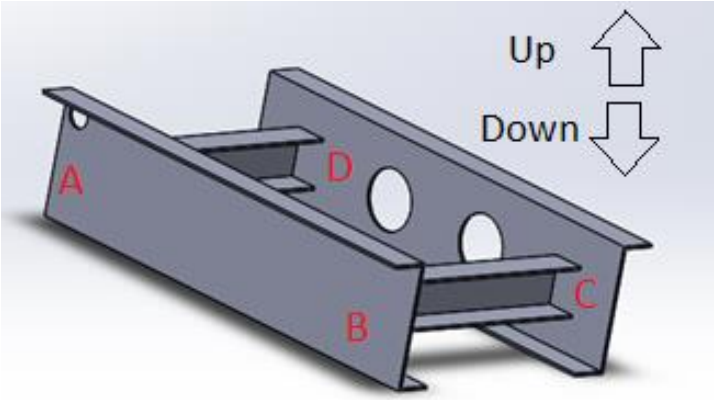

Picture 16. Labeling ends of sample structures in a following manner: A, B, C, D.

The sections of samples that were evaluated to be most prone to LME cracking were examined. Such structures included welds, edges of lightening holes and suspension holes and top and bottom side of bends at the ends of the structures. Before applying magnetic particle ink, surface of areas to be examined were cleaned with adequate cleaning products. Specimen 1 and 2 were cleaned with Bycorest Cleanser C5 and specimen 3 and 4 were cleaned with Bycorest Cleanser C10. Magnetic yoke (Magnaflux corp. Model Y-6) was positioned perpendicular to examined area and then moved 90° in place to examine the same area again. This enabled detection of cracks positioned in every direction. Magnetic particle ink was applied to surface as magnetic yoke was turned on, to allow adequate accumulation of magnetic ink to possible flux leakage positions. Specimen 1 and 2 were examined with magnetic ink Bycorest 101 and Specimen 3 and 4 were examined with magnetic ink Bycorest 14HF. The light of the UV-lamp (Magnaflux UV (A) lamp model ZB 100F) was positioned towards area to be examined and special filtered glasses (Nightsea) were used in examination for enhanced contrast. Clear indications of cracks were not detected and indications resembling to ones detected on crack positions of initial sample pieces were not detected. Indications seemed mostly to be marks from cutting and welding of parts, and variation in surface roughness. Zinc was unevenly layered in some parts of the structure which affected accumulation of magnetic ink.

For follow-up examinations zinc layer was etched off from Sample 3 that was thought to possess a structure most prone to possible LME cracking. Sample 3 was cut with plasma which is a more violent cutting method to structure compared to laser cutting. Sample 3 also had lightening holes with steep angles that were prone to possible LME cracking. Due to time constraints zinc was determined to be etched off only from one

sample. Etching was done with a 16 % HCl solution containing inhibitor due its short etching time. Etching was done in the etching bath of the school laboratory`s hot-dip galvanization line. The part was kept in degreasing alkaline solution for 8 minutes rinsed with water and etched in an inhibited HCl bath for 2 hours. Approximately 500 ml of the inhibitor (Rodine 60) was added to bath to ensure that there would be sufficient amount of the inhibitor to prevent hydrogen from diffusing to steel, possibly causing hydrogen embrittlement. The approximate content of the inhibitor in the bath was 0.5 %. Zinc was successfully completely removed from the immersed area.

After the removal of the zinc layer was completed, areas that were most prone to LME were examined. Clear indications of cracks were not detected by visual inspection or magnetic particle examination. Magnetic particle ink tended to accumulate to lower boundaries of welds due to form of welds. Picture 17 illustrates Sample 3 side A after etching of zinc layer when magnetic particle ink is applied to surface of structure. Pictures illustrating lightening hole, bend and other side of weld of part 3 side A before and after etching of zinc layer are listed in Appendix 5.

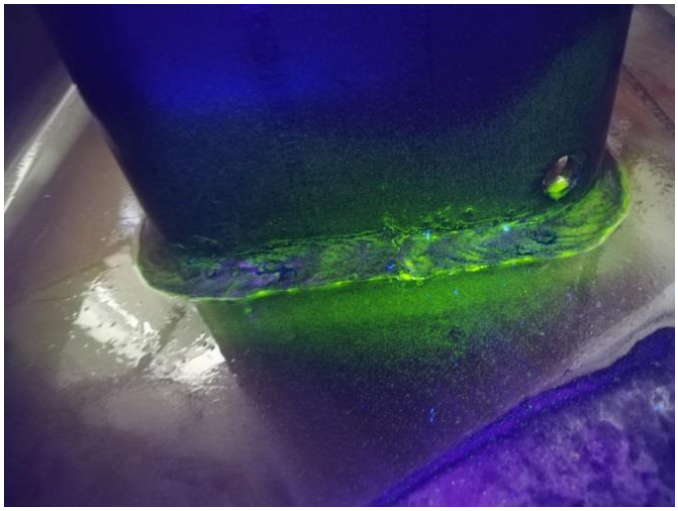

Picture 17. Side A of Sample 6 after the etching of the zinc layer when magnetic particle ink was applied to the surface.

Eddy current inspection was considered to be done to samples, but performing the method would have required noticeable preliminary preparations. Such preliminary preparations would have included manufacturing of equivalent sample pieces and artificial production of cracks reminiscent of LME induced cracks. These actions would have required extra time; therefore, usage of Eddy current inspection method was excluded from this project.

8 Synopsis

In this thesis hot-dip galvanized high strength steel structures were inspected with magnetic particle examination to detect possible cracks induced by liquid metal embrittlement in the hot-dip galvanization process. Determination of suitable methods for the detection of liquid metal induced cracking was conducted. The potential of various solutions regarding etching of zinc was examined.

Clear indications of liquid metal induced cracking were not detected from hot-dip galvanized high strength steel sample structures with visual inspection or magnetic particle inspection. Although cracks were not detected in sample structures, that does not remove the possibility that liquid metal induced cracks could exist. Liquid metal induced cracks may vary in size, therefore being more difficult to be detected. Thickness of examined structures` zinc layer was relatively high, reducing precision of magnetic particle examination. Cracks not induced by liquid metal embrittlement were possible to be detected from under approximately 100 µm thick zinc layer with magnetic particle examination. Etching experiments of zinc were successfully conducted.

Confirmation of tested high strength steel structures withstanding hot-dip galvanization with no detectable liquid metal induced cracking was achieved. Results of high strength steel (yield strength >1100 MPa) withstanding hot-dip galvanization may increase interest for further studies of the material. Results of zinc etching experiments can be used in studies where there is a need for the removal of zinc from hot-dip galvanized steel structures.

References

Applications. NDT resource Center. Internet Source. <https://www.nde-ed.org/EducationResources/CommunityCollege/EddyCurrents/Applications/tubeinspection.htm>. Read 14.5.2019.

Basic Principles. NDT Resource Center. Internet source. <http://www.nde-ed.org/EducationResources/CommunityCollege/MagParticle/Introduction/basicprinciples.htm>. Read 14.5.2019.

Becker W.T., Shipley R.J. 2002. ASM Handbook. Volume 11: Failure Analysis and Prevention, 10th Edition. ASM International.

Beldyk. Richard M. 2014. Inspecting for Galvanization-related Cracking in Steel Structures. Ohio bridge Corp etc. Internet Source. <https://app.aws.org/itrends/2004/07/it0704-29.pdf>. 14.5.2019.

Billur Eren, Altan Taylan, Dukeman Jim. 2014. Three Generations of Advanced High-strength steels for Automotive Applications, Part II. Stamping Journal an FMA Publication. Internet Source. <https://ercnsm.osu.edu/sites/ercnsm.osu.edu/files/uploads/S_FormingAHSS/664-2.pdf>. Read 13.5.2019.

Billur Eren, Altan Taylan. 2013. Three Generations of Advanced High-strength Steels for Automotive Applications, Part I. Stamping Journal an FMA Publication. Internet Source <https://ercnsm.osu.edu/sites/ercnsm.osu.edu/files/uploads/S_FormingAHSS/664-1.pdf>. Read. 13.5.2019.

Billur Eren, Altan Taylan. 2014. Three generations of advanced high-strength steels for automotive applications, Part III. Stamping Journal an FMA Publication. Internet Source. <https://ercnsm.osu.edu/sites/ercnsm.osu.edu/files/uploads/S_FormingAHSS/666-3.pdf>. Read 13.5.2019.

Busse Matthias Prof. Dr.-Ing. Lehmhus Dirk Dr.-Ing. Herrmann Axel S. Prof. Dr. -Ing. Kayvantash Kambiz Prof. Dr. 2013. Structural Materials and Processes in Transportation. Wiley-VCH Verlag GmbH & Co.

Cramer Stephen D. Covino Jr. Bernard S. 2005. ASM Handbook. Volume 13 B: Corrosion Materials. ASM International.

Demeri Mahmoud Y. 2012. Advanced High-Strength Steels: Science, Technology, and Applications. ASM International.

Eddy Current Principle. Kontroll Technik. Internet Source. <http://www.kontrolltechnik.com/methods/eddy-current-principle>. Read 14.5.2019.

Equipment in ENSPL. Internet Source. <http://www.eminentndt.in/ndt-equipment.html#>. Read 14.5.2019.

European General Galvanizers Association (EGGA). 2014 Controlling liquid metal assisted cracking during galvanizing of constructional steelwork.

Historia, SSAB:n Virstanpylväät. Internet Source. <https://www.ssab.fi/ssab-konserni/tietoja-ssabsta/ssab-lyhyesti/historia>. Read in 30.8.2019.

History of Eddy Current Testing. NDT Resource Center. Internet Source. <https://www.nde-ed.org/EducationResources/CommunityCollege/EddyCurrents/Introduction/historyofET.htm>. Read 14.5.2019.

Kauppi Timo, Kesti Vili. 2016. Ultralujat teräkset kestävän kehityksen kärjessä. UAS. Journal. Internet Source. <https://uasjournal.fi/category/4-2016/>. Read 13.5.2019.

Kohlman David G. September 18, 2018. A Review of Recent Advances in the Understanding of Liquid Metal Embrittlement. Los Alamos National Laboratory, New Mexico: Corrosion journal.org.

Lightning. NDT Resource Center. Internet Source. <https://www.nde-ed.org/EducationResources/CommunityCollege/MagParticle/ProcessControl/Lighting.htm>. Read 14.5.2019.

Ling. A. Wang. M. Kong. L. 2018. Liquid Metal Embrittlement of Galvanized Steels During Industrial Processing: A Review. Shanghai Jiao Tong University, Nature Singapore. Pte. Ltd. Internet Source. <http://rwlab.sjtu.edu.cn/tiwm/papers/V1N3-2.pdf>. Read 20.5.2019.

Lippold. John C. 2014. Welding Metallurgy and Weldability. John Wiley & Sons Incorporated.

Lämsä Janne, Kiuru Henri. 2012. Ultralujat rakenne- ja kulutusteräkset - tärkeimmät ominaisuudet suunnittelulle. Raahen Seudun Teknologiakeskus Oy, Oulun yliopisto. Internet Source. <https://docplayer.fi/2416872-Ultralujat-rakenne-ja-kulutusterakset-tarkeimmat-ominaisuudet-suunnittelulle.html>. Read 20.5.2019.

Magnetic Particles. NDT Resource Center. Internet Source. <https://www.nde-ed.org/EducationResources/CommunityCollege/MagParticle/Equipment/Particles.htm>. Read 14.5.2019.

Mechanical Engineering and Metals Industry Standardization in Finland. Rikkomaton aineenkoetus. 2016. Magneettijauhetarkastus. Osa 1: Yleisohjeet. SFS-EN ISO 9934-1:2016. 2016. Internet Source. <https://online.sfs.fi/fi/index/tuotteet/SFS/CENISO/ID2/9/460677.html.stx>. Read 25.7.2019.

Nilsson Karl-Fredrik JRC, Hojna Anna CVR-Rez. 2018. Overview of Mechanisms & Models for Liquid metal Embrittlement and Future Directions. The European Commissions`s science and knowledge service. Internet Source. <http://publications.jrc.ec.europa.eu/repository/bitstream/JRC113457/eur29437en_lme_models_overview_jrc_trrev.pdf>. Read 8.5.2019.

Nygren Ville. 2015. LNT-menetelmä sulametallihaurauden arvioimseen terästen kuumasinkityksessä. Metropolia University of Applied Sciences. Thesis. Internet Source. < https://www.theseus.fi/handle/10024/100475>. Read 35.7.2019.

Portable Magnetizing Equipment for Magnetic Particle Inspection. NDT Resource Center. Internet Source. <http://www.nde-ed.org/EducationResources/CommunityCollege/MagParticle/Equipment/EquipmentPortable.htm>. Read 14.5.2019.

Rajala Janne. 2014. Sulametallihauraus lujien terästen kuumaupotuksessa. Metropolia University of Applied Sciences. Thesis. <Internet Source. https://www.theseus.fi/handle/10024/83965>. Read 25.7.2019.

Ram Sai K.S. 2010. Design of Steel Structures. Pearson Education India.

Schmitt Jean-Hubert, Iung Thierry. 2018. New developments of advanced high-strength steels for automotive applications. <https://www.sciencedirect.com/science/article/pii/S1631070518301166>. Read 14.5.2019.

SHY (Suomen hitaustekniillinen yhdistys) NDT-komitea. NDT-menetelmät: Magneettijauhetarkastus.

SHY (Suomen hitaustekniillinen yhdistys) NDT-komitea. NDT-menetelmät: Pyörrevirtatarkastus.

SSAB. Annual report 2018.

SSAB lyhyesti. <https://www.ssab.fi/ssab-konserni/tietoja-ssabsta/ssab-lyhyesti>. Internet source. Read 30.8.2019.

Teknogoliainfo Teknova Oy 2001. Raaka-ainekäsikirja Muokatut Teräkset. Teknogoliainfo.

Thickness Measurements. NDT Resource Center. Internet Source. <https://www.nde-ed.org/EducationResources/CommunityCollege/EddyCurrents/Applications/thicknessmeasurements.htm>. Read 14.5.2019.

Vermeersch M., De Waele W., Van Caenegem N. 2011. LME Susceptibility of Galvanized Welded Structures of High Strength Steels. Laboratory Soete. Internet Source. Read 14.5.2019.

Appendix 1. Figures of surface thickness and mass of samples during etching experiments

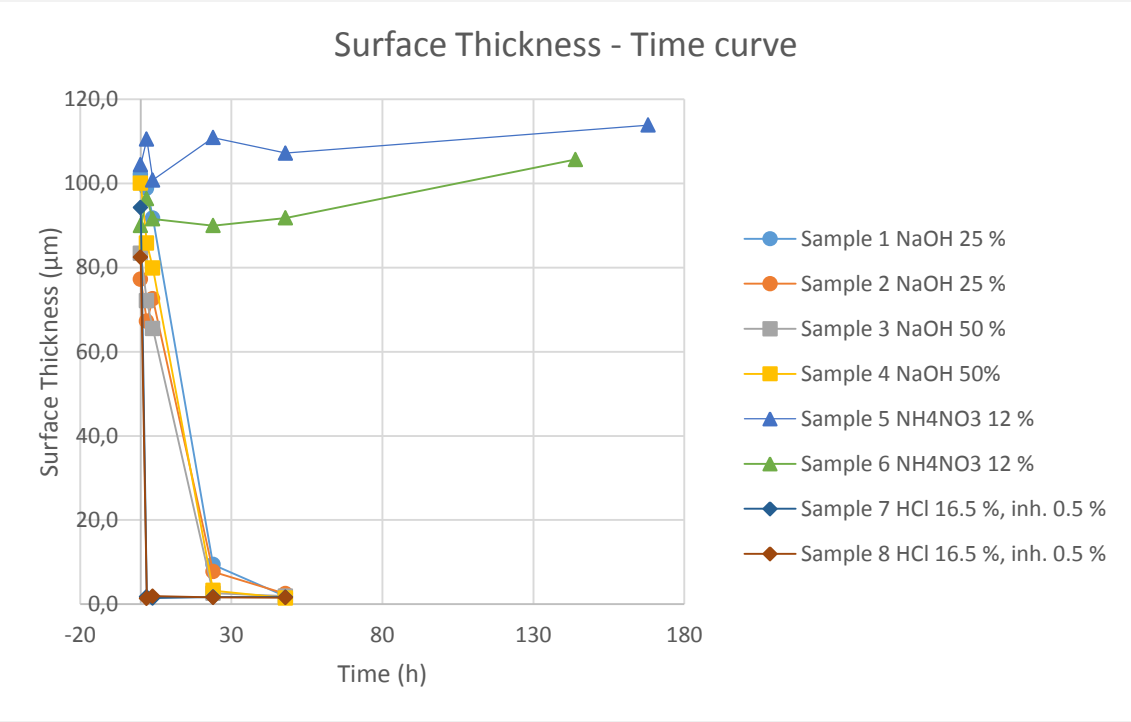

Figure 1.1. Surface thickness - Time curve. Time axis extended to display till 180 h.

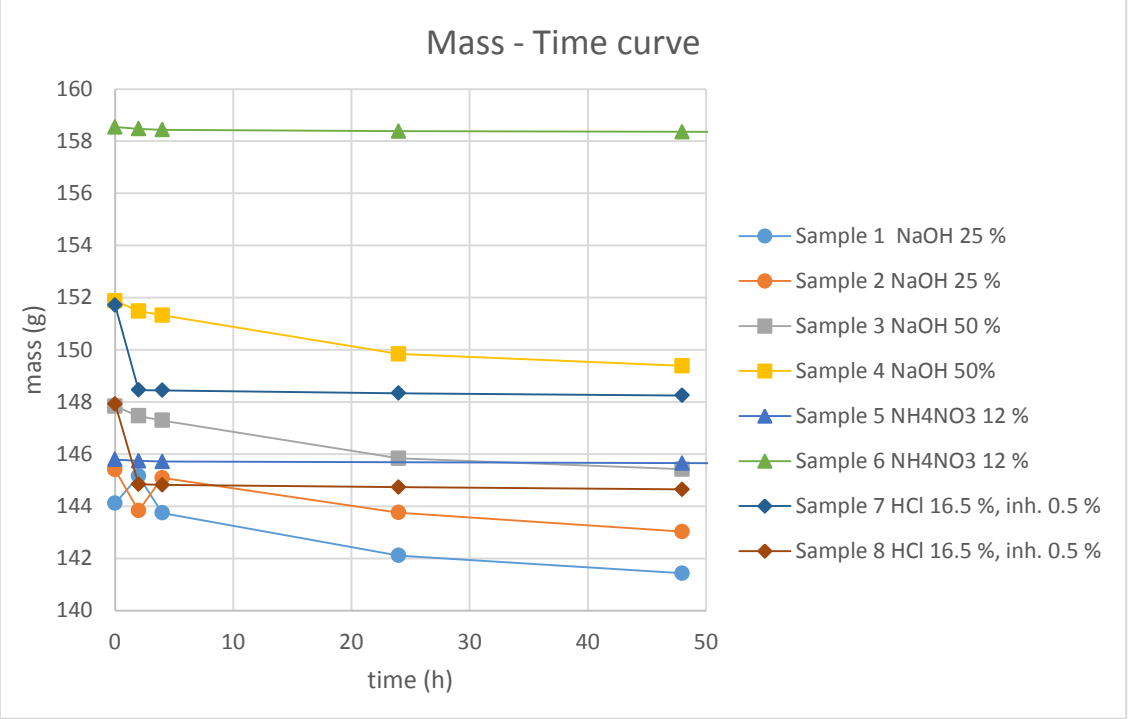

Figure 1.2. Mass - Time curve. Time axis extended to display till 180 h.

Appendix 2. 2-D blueprints of sample structures

Sample 1

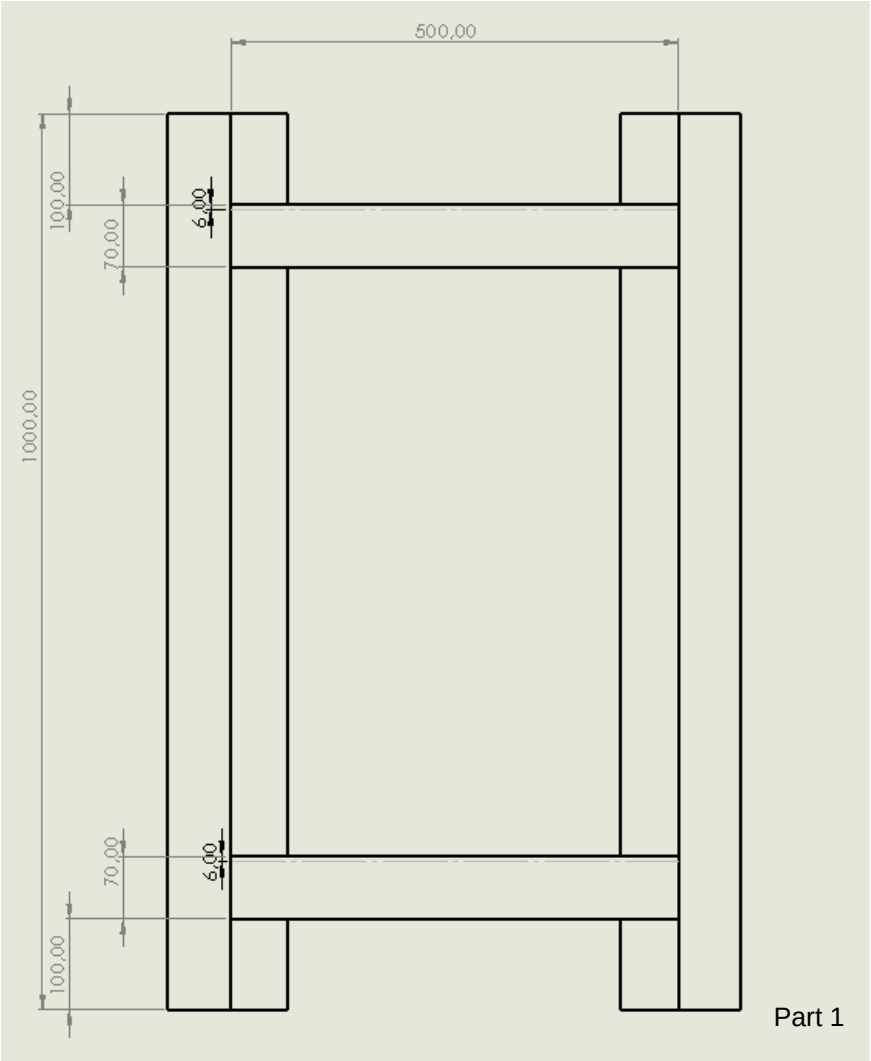

Picture 2.1. Part 1 from above.

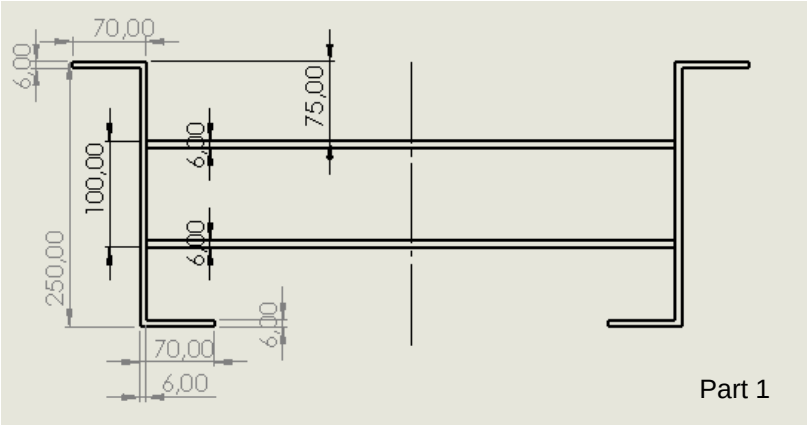

Picture 2.2. Part 1 from the front.

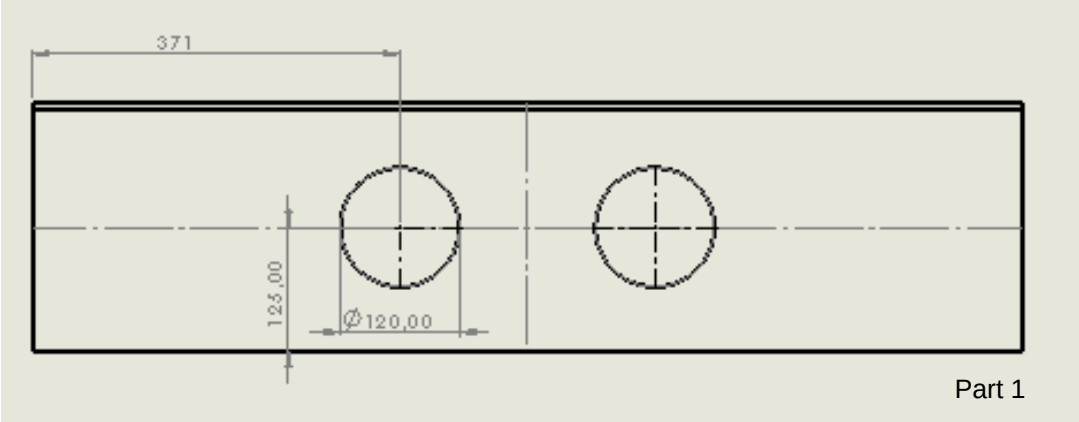

Picture 2.3. Part 1 from the right.

Picture 2.4. Part 1 from the left.

Sample 2

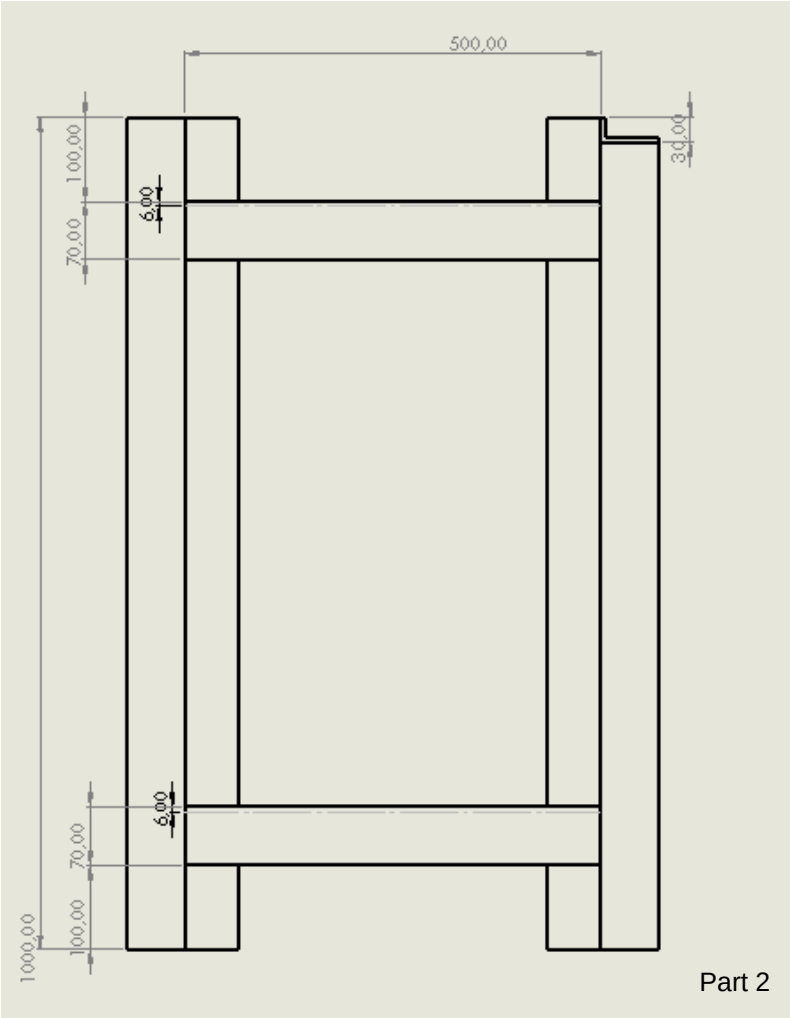

Picture 2.5. Part 2 from above.

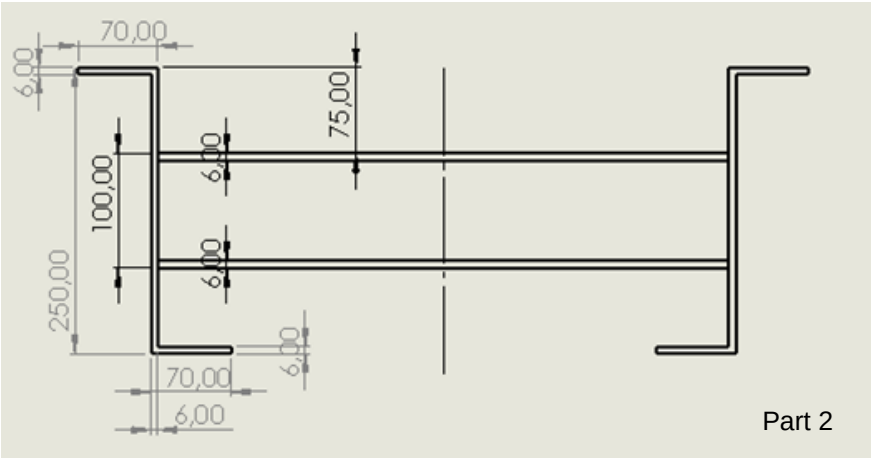

Picture 2.6. Part 2 from the front.

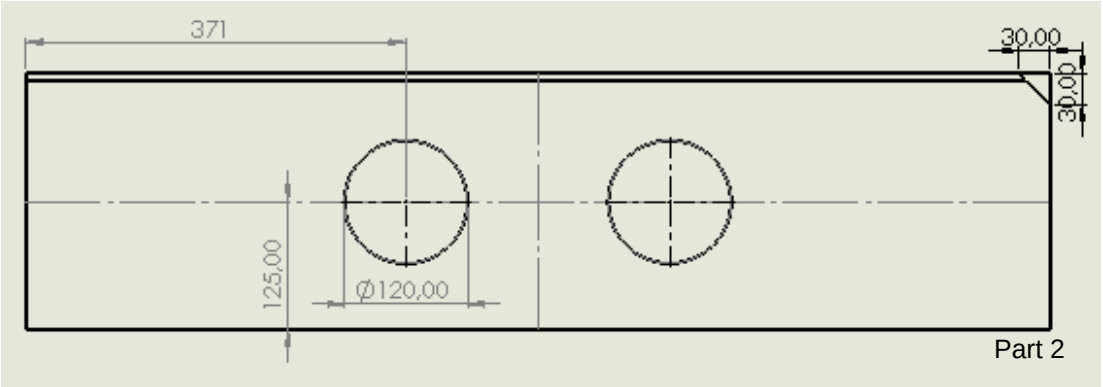

Picture 2.7. Part 2 from the right.

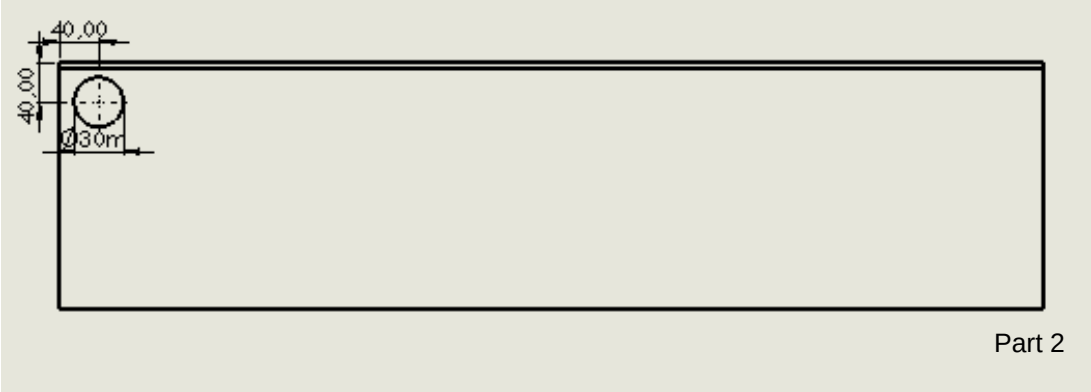

Picture 2.8. Part 2 from the left.

Sample 3

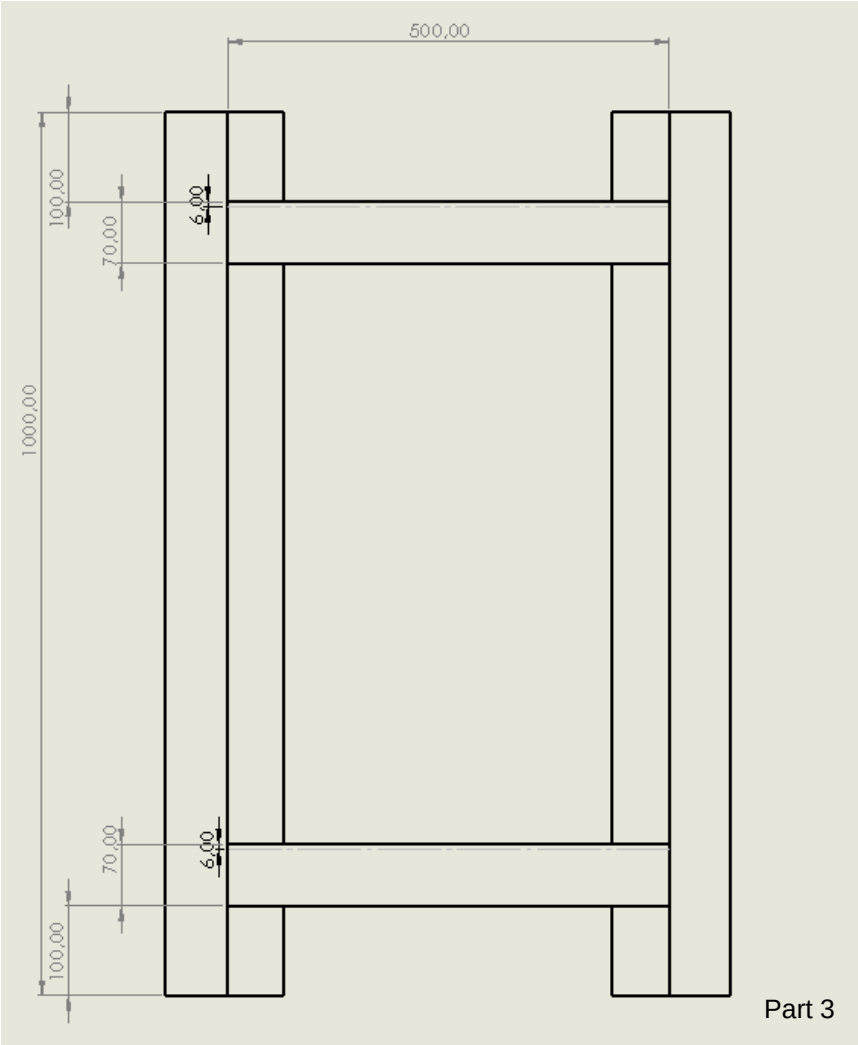

Picture 2.9. Part 3 from above.

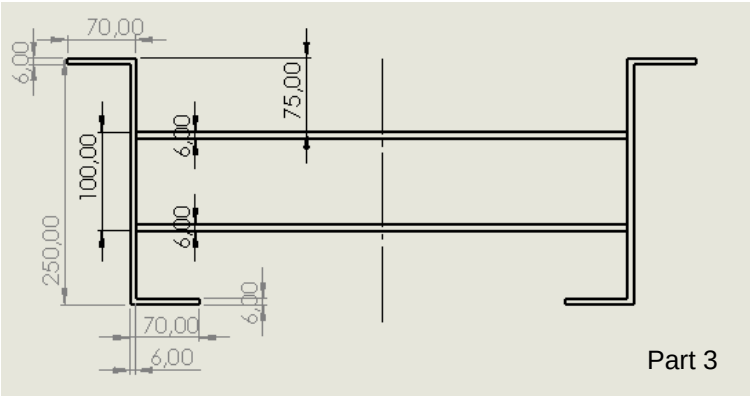

Picture 2.10. Part 3 from the front.

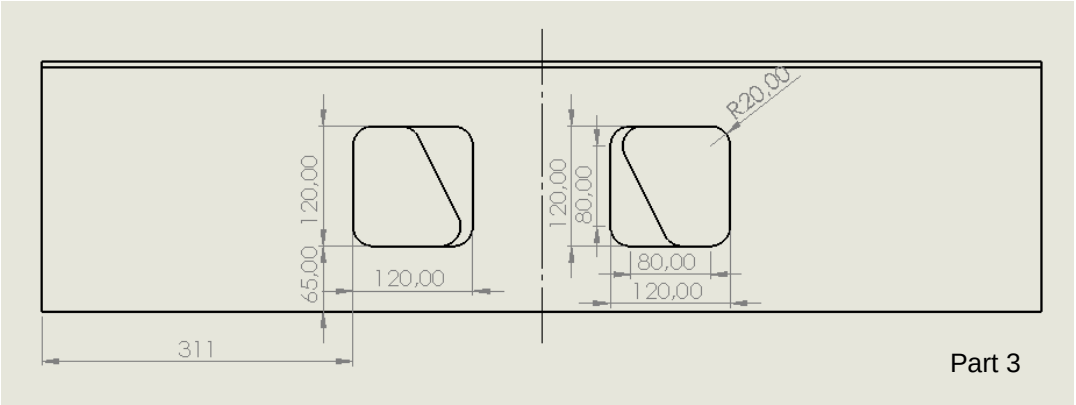

Picture 2.11. Part 3 from the right.

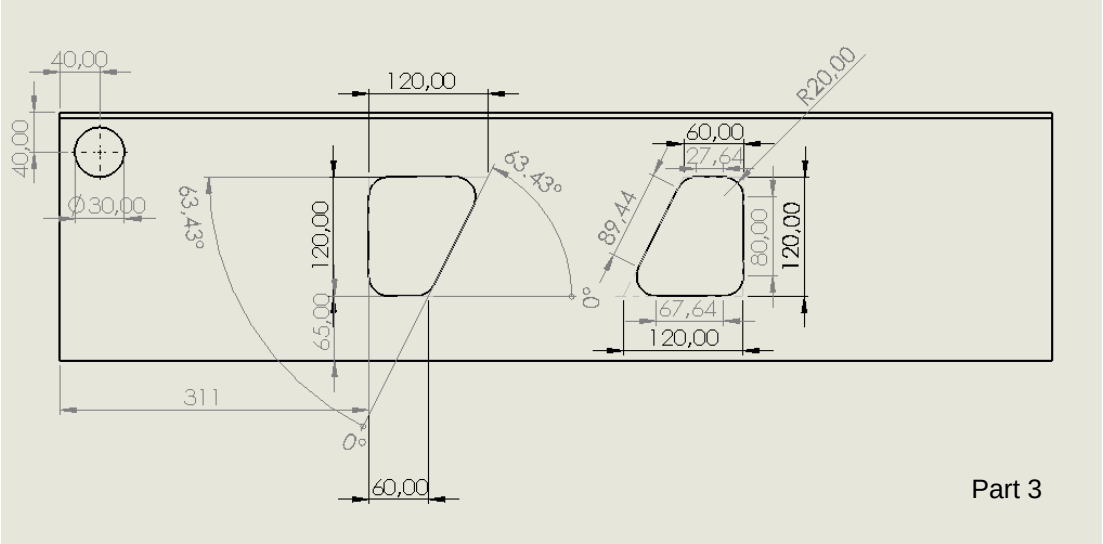

Picture 2.12. Part 3 from the left.

Sample 4

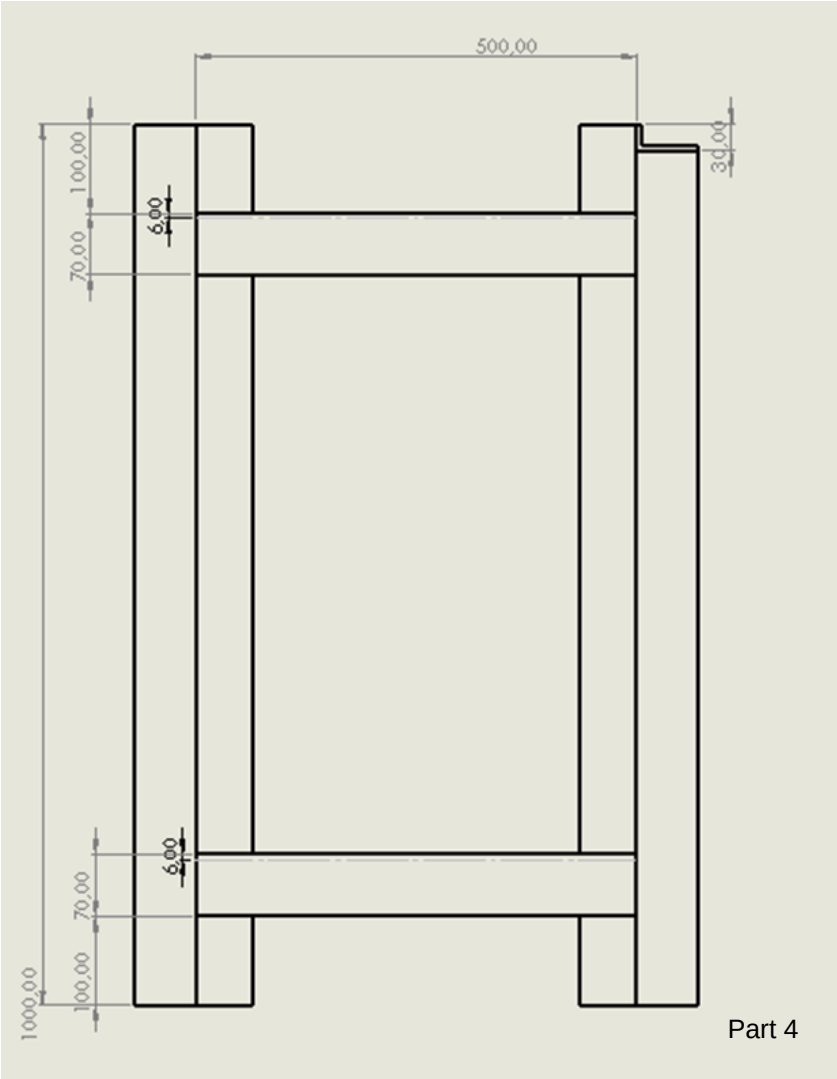

Picture 2.13. Part 4 from above.

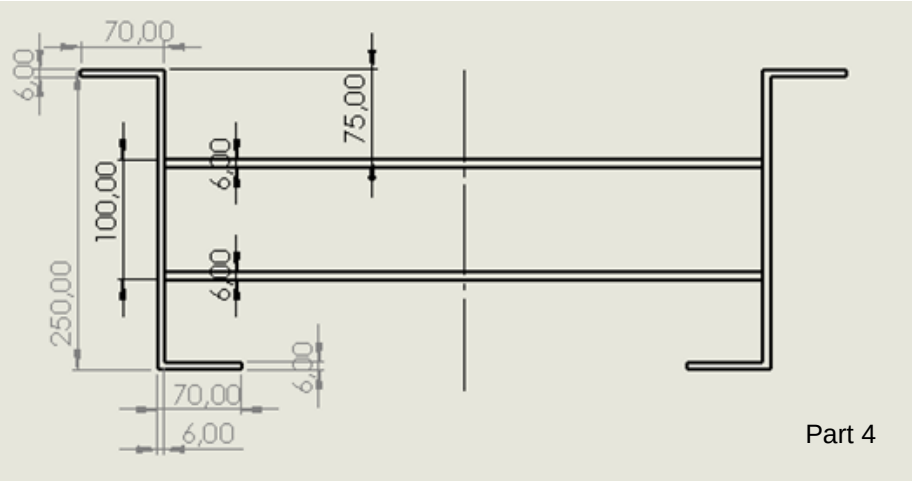

Picture 2.14. Part 4 from the front.

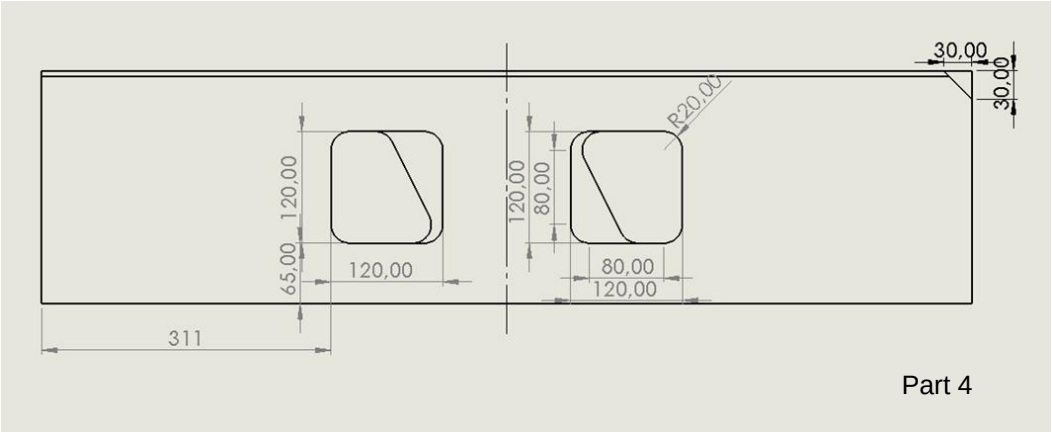

Picture 2.15. Part 4 from the right.

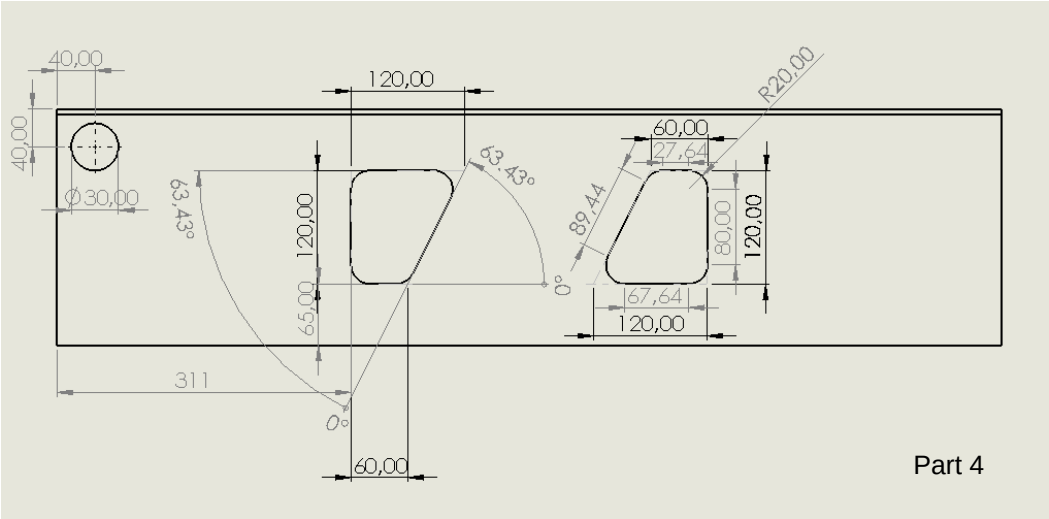

Picture 2.16. Part 4 from the left.

Appendix 3. Spread blueprints of sample pieces

Manufacturing quantities of pieces

Middle bar	8 pieces
Part 1 right side	1 pieces
Part 2 right side	1 pieces
Parts 1 and 2 left side	2 pieces
Part 3 right side	1 pieces
Part 4 right side	1 pieces
Parts 3 and 4 left side	2 pieces
Altogether:	16 pieces

Middle bar

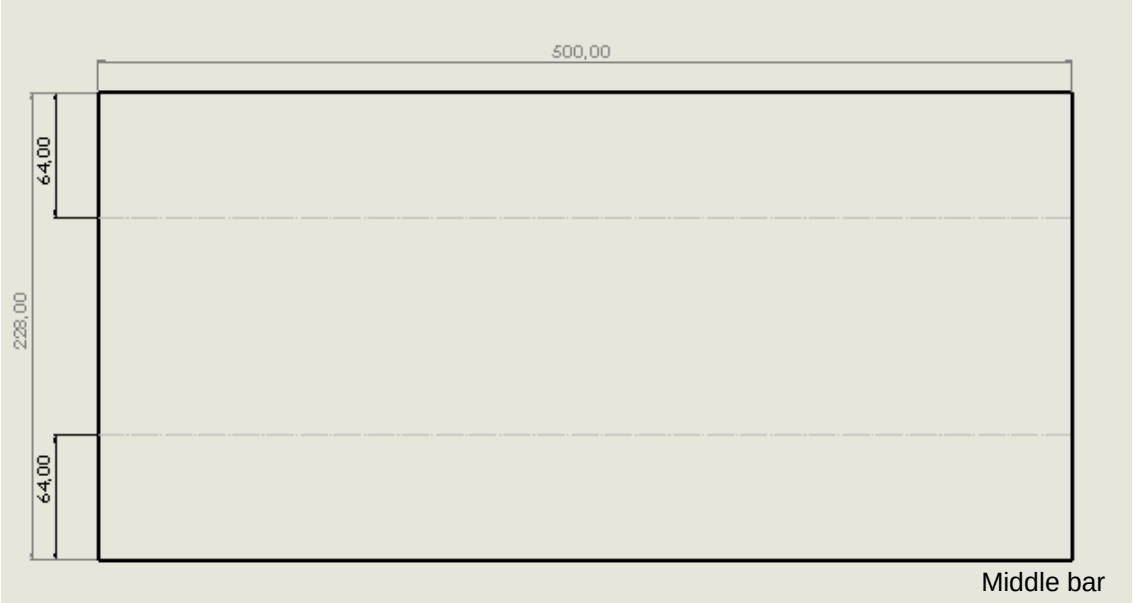

Picture 3.1. Middle bar (8 pieces).

Samples 1 and 2

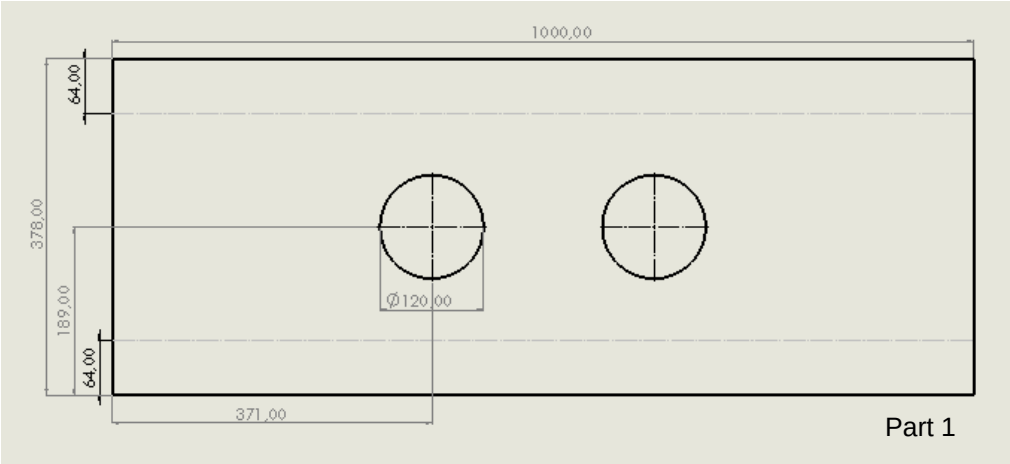

Picture 3.2. Part 1 from the right (1 piece).

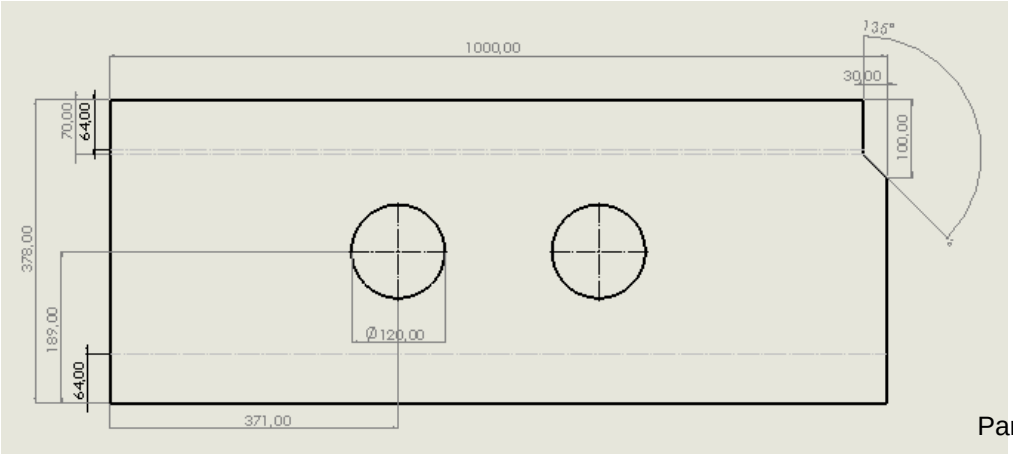

Picture 3.3. Part 2 from the right (1 piece).

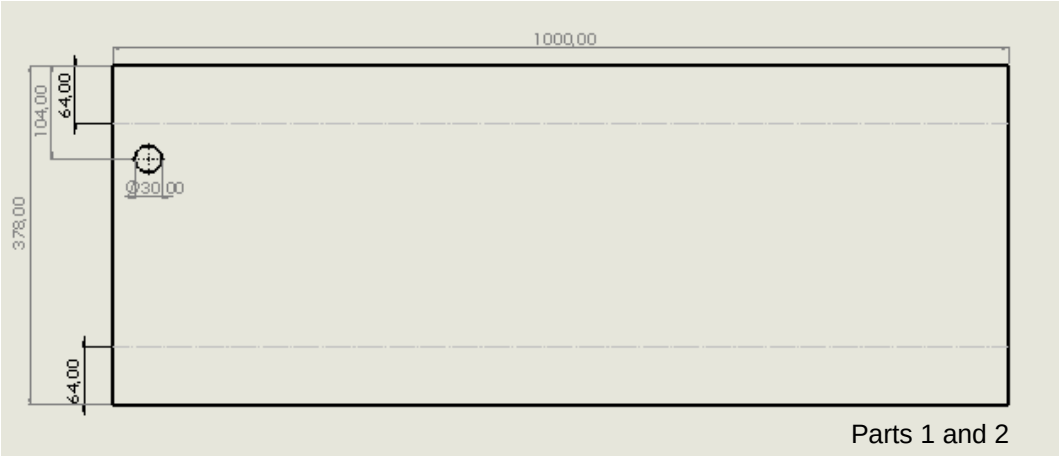

Picture 3.4. Parts 1 and 2 from the left (2 pieces)

Samples 3 and 4

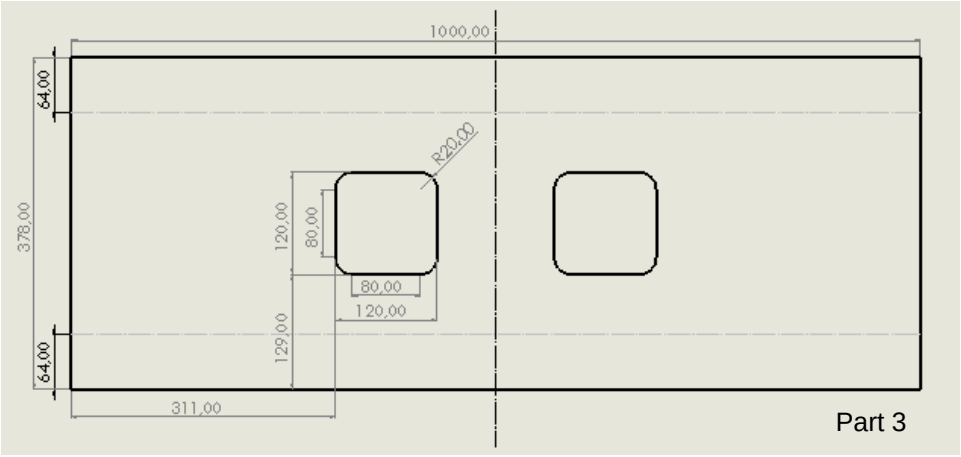

Picture 3.5. Part 3 from the right (1 piece).

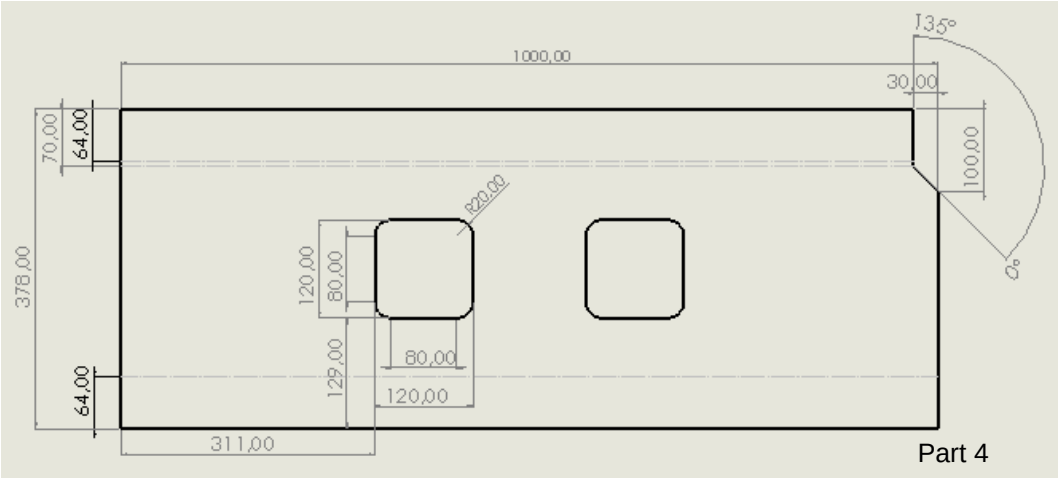

Picture 3.6. Part 4 from the right (1 piece).

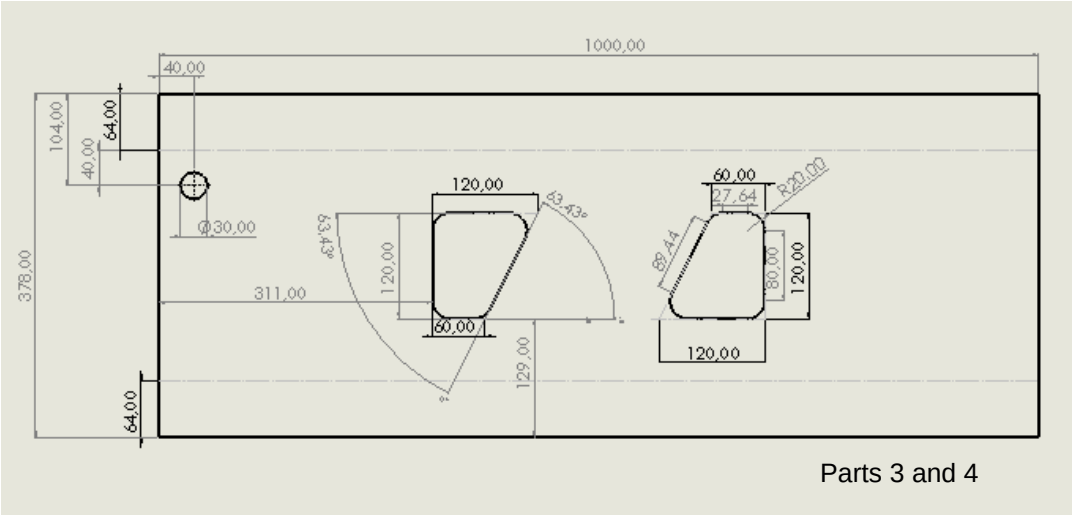

Picture 3.7. Parts 3 and 4 from the left (2 pieces).

Appendix 4. Surface thickness measurements of zinc layer after hot-dip galvanization

Table 4.1. Surface thickness measurements of zinc layer of Sample 3 after hot-dip galvanization.

measurement	surface thickness (µm)
1	110
2	90.7
3	107
4	108
5	87
6	108
7	86.3
8	113
9	110
10	107
average	102.7

Appendix 5. Pictures illustrating Sample 3 before and after etching of zinc layer

Picture 5.1. Lightening hole of Sample 3 before etching of zinc layer.

Picture 5.2. Lightening hole of Sample 3 after etching of zinc layer.

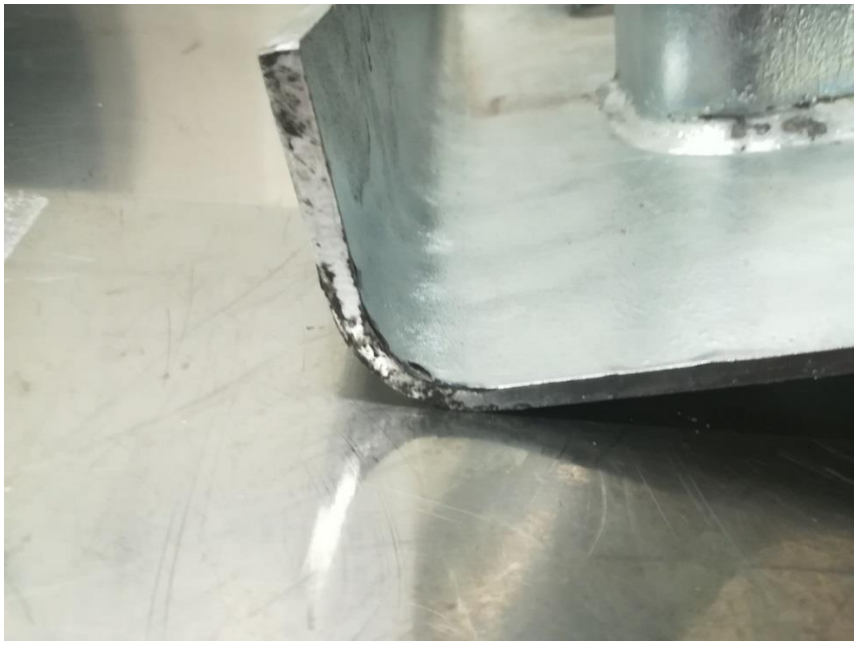

Picture 5.3. Bend of Sample 3 before etching of zinc layer.

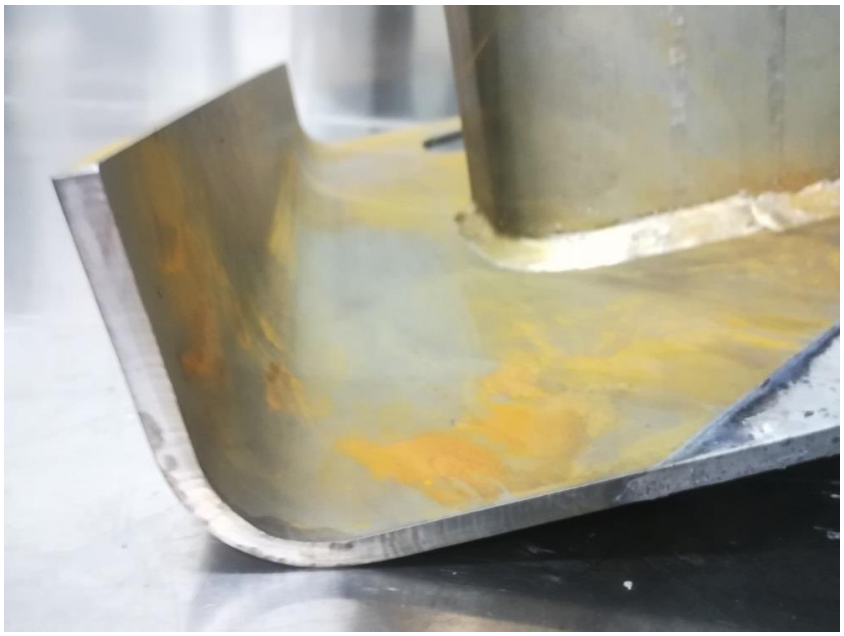

Picture 5.4. Bend of Sample 3 after etching of zinc layer.

Picture 5.5. Weld of Sample 3 before etching of zinc layer.

Picture 5.6. Weld of Sample 3 after etching of zinc layer.